

LATERAL COMPRESSION OF HOMOPOLYMERS AND  
COPOLYMERS AT THE AIR-LIQUID INTERFACES  
FOR GOOD SOLVENTS

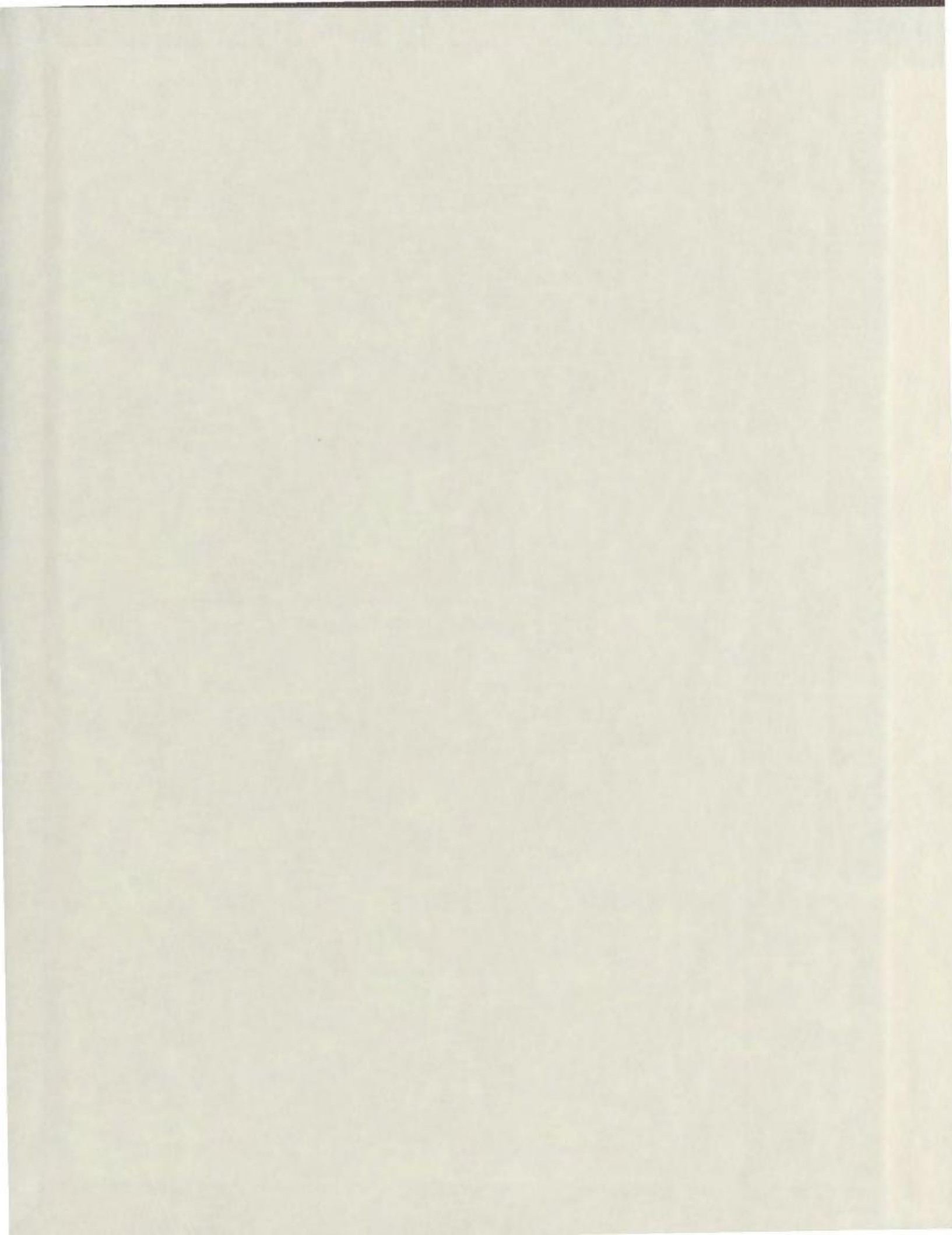
CENTRE FOR NEWFOUNDLAND STUDIES

---

**TOTAL OF 10 PAGES ONLY  
MAY BE XEROXED**

(Without Author's Permission)

IYAD M. ABU-AJAMIEH







National Library  
of Canada

Bibliothèque nationale  
du Canada

Acquisitions and  
Bibliographic Services

Acquisitions et  
services bibliographiques

395 Wellington Street  
Ottawa ON K1A 0N4  
Canada

395, rue Wellington  
Ottawa ON K1A 0N4  
Canada

*Your file* *Votre référence*

*ISBN: 0-612-93008-4*

*Our file* *Notre référence*

*ISBN: 0-612-93008-4*

The author has granted a non-exclusive licence allowing the National Library of Canada to reproduce, loan, distribute or sell copies of this thesis in microform, paper or electronic formats.

L'auteur a accordé une licence non exclusive permettant à la Bibliothèque nationale du Canada de reproduire, prêter, distribuer ou vendre des copies de cette thèse sous la forme de microfiche/film, de reproduction sur papier ou sur format électronique.

The author retains ownership of the copyright in this thesis. Neither the thesis nor substantial extracts from it may be printed or otherwise reproduced without the author's permission.

L'auteur conserve la propriété du droit d'auteur qui protège cette thèse. Ni la thèse ni des extraits substantiels de celle-ci ne doivent être imprimés ou autrement reproduits sans son autorisation.

---

In compliance with the Canadian Privacy Act some supporting forms may have been removed from this dissertation.

Conformément à la loi canadienne sur la protection de la vie privée, quelques formulaires secondaires ont été enlevés de ce manuscrit.

While these forms may be included in the document page count, their removal does not represent any loss of content from the dissertation.

Bien que ces formulaires aient inclus dans la pagination, il n'y aura aucun contenu manquant.

**Canada**



**Lateral Compression of Homopolymers and  
Copolymers at the Air-Liquid Interfaces for Good  
Solvents**

by

© Iyad M. Abu-Ajamieh  
B.Sc. (1990) University of Jordan

A thesis submitted to the  
School of Graduate Studies  
in partial fulfillment of the  
requirements for the degree of  
Master of Science.

Department of Physics and Physical Oceanography  
Memorial University of Newfoundland

August 11, 2003

ST. JOHN'S

NEWFOUNDLAND

# Contents

---

<b>Abstract</b>	<b>v</b>
<b>Acknowledgements</b>	<b>vii</b>
<b>List of Tables</b>	<b>viii</b>
<b>List of Figures</b>	<b>x</b>
<b>1 Introduction</b>	<b>1</b>
1.1 General Remarks . . . . .	1
1.2 Polymers in Solution . . . . .	2
1.3 Polymers at Surfaces . . . . .	3
1.3.1 Adsorbed Homopolymers . . . . .	4
1.3.2 End-Tethered Polymers . . . . .	4
1.3.3 Applications of Polymers at Surfaces . . . . .	7
1.4 Analytic Theories of Polymers at Surfaces . . . . .	8
1.4.1 Scaling Theory . . . . .	9
1.4.2 Mean Field Theories . . . . .	12
1.4.3 Diblock Copolymer Adsorption . . . . .	15

1.5	Experimental Studies of End-Tethered Polymers . . . . .	17
1.6	Numerical Models . . . . .	20
1.7	Objective and Outline of this Work . . . . .	24
<b>2</b>	<b>Numerical Self-Consistent Field Theory</b>	<b>26</b>
2.1	Introductory Remarks . . . . .	26
2.2	Partition Function . . . . .	29
2.3	The Saddle Function Method: Mean Field Approximation . . . . .	34
2.4	Self-consistent Mean Field Theory of Tethered Polymer . . . . .	35
<b>3</b>	<b>Lateral Compression - Excess Surface Pressure</b>	<b>41</b>
3.1	Introduction . . . . .	41
3.1.1	Experimental Studies on the Lateral Compression of Copoly- mers at the Air-Liquid Interface . . . . .	42
3.2	Numerical Self-Consistent-Field Approach . . . . .	45
3.2.1	The Homopolymer Spread as a Monolayer . . . . .	46
3.2.2	Diblock Copolymer at the Air-Liquid Interface . . . . .	48
3.2.3	The Model of the Interaction with the Surface . . . . .	51
3.2.4	Free Energy of the System, Interfacial Tension and Surface Pressure . . . . .	52
3.2.5	Approximations in Earlier nSCF Calculations . . . . .	56
3.3	Results and Discussion . . . . .	56
3.3.1	Surface Pressure Isotherms - Homopolymer . . . . .	58
3.3.2	Surface Pressure Isotherms - Copolymer . . . . .	63
3.4	Surface Pressure Excess . . . . .	64

3.5	Surface Pressure Contributions . . . . .	68
3.6	Comparison with Earlier nSCF Calculations . . . . .	69
<b>4</b>	<b>Concluding Remarks</b>	<b>73</b>
4.1	Summary of the Results . . . . .	73
4.2	Future Work . . . . .	76

# Abstract

End-tethered polymer layers are formed when a collection of polymers is anchored by one end to a surface, with the remainder dangling into solvent. These systems have been studied extensively both experimentally and theoretically, and numerical self-consistent field (nSCF) theory can now explain much of their structure and physical behavior very well. However, the surface pressure is not yet understood.

Bijsterbosch *et al.* performed experiments in which they examined a series of polystyrene-poly(ethylene ) (PS-PEO) diblock copolymers at the air-water interface with varying length of PEO block. They found that surface pressure excess varies smoothly and slowly with polymer density. On the other hand, Kent *et al.* investigated systems of diblock copolymer poly(dimethylsiloxane-styrene) (PDMS-PS) spread as a monolayer at the free surface of ethyle benzoate (EB). In these systems PDMS lies flat on the top of EB, with PS dangling into EB which is a good solvent for PS. They reported that surface pressure excess varies smoothly and slowly at low density, then quickly at high density.

All theoretical treatments except one give weak variation similar to observations of Bijsterbosch and coworkers. The exception is the nSCF calculation of Baranowski. In this thesis, nSCF calculations have been performed to examine Baranowski's work, and to model Kent's experiments. The results are in good agreement with predictions of the scaling theories for the surface pressure isotherms, which are also compatible

with experimental measurements performed by Bijsterbosch *et al.*

# Acknowledgements

I express my sincere appreciation to all who helped me in any way in doing this work. I wish to express my deep gratitude to my supervisor Dr. Mark D. Whitmore for his support, encouragement, and for giving me the opportunity to work with him. His unbelievable help, deep understanding, inspired me and gave me the strength to go forward in this thesis.

I also wish to express my thanks to Dr. Baranowski for his permission to use his code, most of it written using Fortran 77, which enables me to go through this work.

It is a great pleasure to thank the School of Graduate Studies for their generous financial support, and Department of Physics for providing me with all facilities needed to accomplish this work.

I would like to thank Fred Perry, and Darryl Reid for fruitful expertise, which enabled me to overcome the difficulties that I faced in my work.

I also wish to express my warm thanks to my friends, Abdel-Rahman, Nidal, Saleh, David, Mahmoud, Mohammad, and Hesham, for their wonderful support and constant encouragement.

I am grateful to my parents and my brothers for their love, support, and care.

St. John's, NL, Canada, June 2003

Iyad M. Abu-Ajamieh

# List of Tables

3.1 Polymers used in the calculations. The polymers are labeled by the block molecular weights, in kg/mol, of the PDMS and PS blocks respectively. . . . .	64
--	----

# List of Figures

1.1	Polymer chains attached by one end to nonadsorbing surface. Mushroom (a) and brush (b) regimes. The brush height is $h$ . The details of this figure relate to the scaling theory discussed in section 1.5.1 . . . .	6
1.2	Illustration of the monolayer system formed by PDMS-PS diblock copolymer on EB . . . . .	19
1.3	Two regimes for surface pressure excess, $\Delta\pi$ as a function of the number of chains per unit area for the 28-330 PDMS-PS copolymer. The solid line is fitted to the calculations done by Baranowski. While the dashed line is the line of the best fit of 5/3 power law dependence. . . . .	23
3.1	Surface pressure $\pi$ as a function of the number of adsorbed chains per unit area for PDMS homopolymers, $M_w = 25,000$ and $M_w = 50,000$ . (The lines are guides to the eye). . . . .	59
3.2	Surface pressure $\pi$ as a function of the number of adsorbed monomers per unit area for PDMS homopolymers with $M_w = 25,000$ and $M_w = 50,000$ . . . . .	60

3.3	Density profiles for PDMS homopolymer with $M_w = 25,000$ for different values of the surface coverages. The surface coverage, $\Sigma$ , is expressed in units of $\text{nm}^2$ , and the adsorbed amount $\Gamma$ in numbers of adsorbed monomers per $\text{nm}^2$ . . . . .	61
3.4	Surface pressure $\pi$ as a function of the surface concentration, $1/\Sigma$ . The polymers are labeled by the block molecular weights in $\text{kg/mol}$ , of the PDMS and PS blocks, respectively. . . . .	63
3.5	Comparison of surface pressure, $\pi$ as a function of the adsorbed PDMS monomers, for the diblock copolymer with homopolymer. The polymers are labeled by the block molecular weights in $\text{kg/mol}$ , of the PDMS and PS blocks, respectively. $T=300\text{K}$ as the ambient temperature was used to express the pressure in the units of $[\text{mN/m}]$ . . . . .	65
3.6	Surface pressure excess, $\Delta\pi$ , as a function of the number of chains per unit area $1/\Sigma$ . . . . .	66
3.7	Surface pressure excess, $\Delta\pi$ , as a function of the number of chains per unit area $1/\Sigma$ , on a double-logarithmic scale for different copolymers. The dashed line is the line of the best fit using an assumed exponent power law dependence. . . . .	67
3.8	The contribution $\pi_{ext}$ to the surface pressure $\pi$ as a function of the number of PDMS monomers per unit area adsorbed onto the surface. . . . .	69
3.9	The contribution $\pi_{int}$ to the surface pressure $\pi$ as a function of the number of PDMS monomers per unit area adsorbed onto the surface. . . . .	70
3.10	The contribution $\pi_{ent}$ to the surface pressure $\pi$ as a function of the number of PDMS monomers per unit area adsorbed onto the surface. . . . .	71

# Chapter 1

## Introduction

### 1.1 General Remarks

Polymer science is a typical multi-disciplinary subject, with increasing influence on our lives. All substances referred to as polymers, or macromolecules, are giant molecules with molar masses ranging from several thousands to several millions. Because of the diversity of functions and structures, macromolecules have been grouped under two major categories, natural and synthetic. In both cases, the molecules are constructed from structural units called monomers, which are covalently bonded together. When only one type of monomer is used, the product is called a homopolymer: on the other hand, if two or more types of monomers are used, the result is known as a copolymer. Both of those kinds of polymers can be linear or branched [1]. The number of monomers is called the degree of polymerization, and it can affect the properties of polymers.

The behavior and the structure of polymers adsorbed onto surfaces from solution are important and have been studied extensively, both experimentally [2 - 25,95 -101] and theoretically [26 - 70]. Properties of polymer systems near surfaces and interfaces

are of increasing importance in many technological and biological applications. Stabilization of colloidal suspensions, blends, lubrication, adhesion, tailoring the bending of biomembranes, and biomedical uses like extending lifetimes of delivery vehicles in the blood stream - all of which are of great importance - represent promising aspects of polymer adsorption.

## 1.2 Polymers in Solution

An arbitrary polymer molecule may or may not dissolve in an arbitrary solvent. The quality of the solvent can be specified by the affinity that exists between the monomers of the chain molecules and the solvent molecules, or in other words the interactions between polymer monomers and solvent molecules. These interactions are responsible for classifying solvents as good, poor and  $\Theta$  solvents, according to the ability of a polymer of infinite molecular weight to be dissolved.

One can think of three effects associated with solution:

1. There are monomer-solvent interactions. The effective interactions are normally repulsive.
2. However, there is an important effect due to the mixing of polymer chains and solvent molecules: the entropy of mixing increases when a solution forms. This increase can overcome the repulsive interactions between the polymer and solvent.
3. The configurational entropy of the chains is a maximum when the chains are described by random walks. If a good solvent penetrates into the chains, then they expand. This reduces the number of configurations available to the chains. As a consequence of this, the entropy of configuration of the system decreases.

In a good solvent, the net decrease in the free energy due to the increase in entropy exceeds the increase due to the interactions, and the polymer dissolves. In

poor solvent the net increase in the internal energy overcomes the entropic effects, and the polymer does not dissolve. If there is a balance between energy and entropic effects, we have a  $\Theta$  solvent.

Any measurement on polymer systems involves contributions from many molecules in a variety of conformations. An important property of polymers is the radius of gyration of the molecule,  $R_g$ , which is a measure of the average size of a molecule. For a given type of molecule in a given environment,  $R_g$  scales as

$$R_g \propto bZ^\nu \quad , \quad (1.1)$$

where  $Z$  is the degree of polymerization, the value of  $\nu$  depends on the polymer's environment, and  $b$  is called the mean statistical segment length.

Polymers in  $\Theta$  solvent can be described by random walks, in which case the radius of gyration scales as  $\sim Z^{1/2}$ . On the other hand, for good solvent polymer chains can be described by self-avoiding random walk, and here  $R_g \sim Z^{3/5}$ . In poor solvent, the exponent in Eq.(1.1) reduces to  $\nu \approx 1/3$ .

### 1.3 Polymers at Surfaces

One can distinguish between two kinds of surfaces, solid and liquid. The conformational and thermodynamic behavior of chain molecules at a surface depends, among other things, on the quality of the solvent and the surface-polymer interactions [47]. If the polymer molecules show a tendency to aggregate near a surface, the surface is said to be attractive and an adsorption layer will form. On the contrary, if the surface is repulsive then the polymer molecules exhibit a depletion region near the surface and the chains remain in solution. In some cases, the effects of the surface are neutral. In general, the range of these interactions can be short or long-range,

and this affects the types of conformations near surfaces or interfaces.

### 1.3.1 Adsorbed Homopolymers

When a solution of polymer chains is in contact with a surface, one can expect that, when each monomer can adsorb at the surface, the polymer sticks to the wall and cannot be desorbed by washing with the pure solvent. At low surface concentrations when neighboring adsorbed chains do not overlap, the conformation of the macromolecules is well-determined by the value of adsorption energy of each monomer [27]. Increasing the surface coverage will introduce other factors which affect the structure of the adsorbed layer, such as monomer concentration, chain flexibility, and polymer-solvent interaction, as well as the molecular weight of the chains.

When a polymer adsorbs on a surface, only part of it makes contact with it. The structure of an adsorbed layer is described in terms of “trains”, “loops” and “tails” [71]. A train is a series of consecutive segments, all in contact with the surface. A loop is constructed from segments all extended into the solvent; it is bound by a train on each side. A tail is terminally bound to a train; the outer end dangles into the solution. In the case of interacting layers adsorbed on two neighbouring surfaces, sections can form bridges [69].

Theoretical study of the behavior of these systems can be technologically important and, furthermore, it enables the explanation of experiments [8, 12, 20] as well provides the ability to predict the physical behavior of systems under investigation.

### 1.3.2 End-Tethered Polymers

When one end of each polymer chain is strongly attached to the surface, but the surface is otherwise repulsive or neutral, an end-tethered polymer layer is formed.

End-anchored polymer layers are obtained in two ways, either by chemical grafting or by diblock copolymer adsorption. The latter case depends very strongly on the quality of solvent for each block of copolymer. Depending on the interaction parameters between solvent molecules and both blocks of the copolymer, one can distinguish between two types of solvent: non-selective and selective. If these interactions between the solvent molecules and both blocks are the same, the solvent is called non-selective. Here, one block adsorbs onto the surface, while the other block dangles into the solvent.

For a non-selective solvent, the solvent penetrates into the adsorbed layer. This adsorbed layer can be treated in a similar way as an adsorbed homopolymer. On the other hand, the dangling block which is called the “buoy” block, is often handled as an end-grafted homopolymer [36]. This treatment can be applied for either selective or non-selective solvent.

The physical structure of the adsorbed layer is characterized by the density profile of each block, thickness of the layer, the adsorbed amount,  $\Gamma$ , which is defined as the total number of monomers per unit area which belong to the adsorbed layer, as well as free energy of the system. Most analytical and numerical procedures focus on the Helmholtz free energy,  $F$ . Usually it is expressed as a sum of two contributions - the interaction energy, which represents the interactions among all components of the system in addition to the interaction with the surface, plus the entropic contribution.

Within this approach, the surface tension  $\gamma$  can be calculated using

$$\gamma = \left( \frac{\partial F}{\partial \mathcal{A}} \right)_{T, V, N_\kappa}, \quad (1.2)$$

where  $\mathcal{A}$  is the total area of the interface,  $T$  is the temperature,  $V$  is the volume of the system and each  $N_\kappa$  is the number of molecules of species  $\kappa$  present in the system.

The primary factors which determine the physical properties of dangling blocks

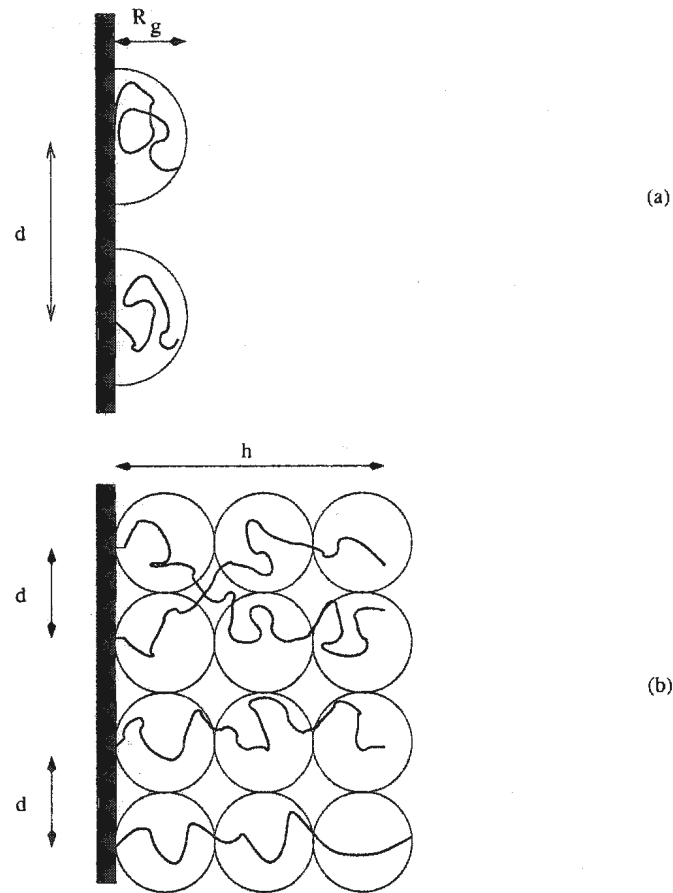


Figure 1.1: Polymer chains attached by one end to nonadsorbing surface. Mushroom (a) and brush (b) regimes. The brush height is  $h$ . The details of this figure relate to the scaling theory discussed in section 1.5.1

are the degree of polymerization of that block,  $Z$ , the quality of the solvent, and the average area per tethered molecule,  $\Sigma$ . It is practical to introduce the reduced surface concentration,  $\sigma^*$ , defined by

$$\sigma^* = \frac{\pi R_g^2}{\Sigma}, \quad (1.3)$$

where  $R_g$  is the radius of gyration of an unperturbed dangling block of polymer in the solvent. Since

$$\Sigma \sim \pi d^2, \quad (1.4)$$

this implies that

$$\sigma^* \sim \left( \frac{R_g}{d} \right)^2, \quad (1.5)$$

where  $d$  is the average distance between grafted sites on the surface. To within a numerical factor,  $\sigma^*$  is the ratio of the cross sectional area of unperturbed dangling block of polymer molecule in solution to the average area associated with it in the grafted state. Values of this ratio can be used to identify two well-known limits of grafted macromolecules. These two limits are schematically presented in figure 1.1.

In the first,  $\sigma^* \ll 1$ , the average distance between anchoring sites is greater than  $R_g$ . This low limit of  $\sigma^*$  describes isolated chains, with no overlap. Each isolated chain occupies roughly a half-sphere with radius comparable to  $R_g$ . This limit is known as the “mushroom regime” [30].

If the number of end-grafted polymers per unit area is high, the chains stretch normal to the planar surface. This stretching restricts the configurations available to the polymer, and the entropy of the system decreases. This interplay between the entropy loss due to stretching and the steric interactions determines the equilibrium layer thickness. The result is a thick layer, a so-called brush [28]. This limit is associated with  $\sigma^* \gg 1$ . In this regime, overlapped coils stretch away from the surface, and the conformations in good solvents are determined by excluded-volume. In terms of the average area per adsorbed molecule,  $\Sigma$ , this limit can be written as

$$\pi R_g^2 \gg \Sigma, \quad (1.6)$$

or, equivalently,  $d \ll R_g$ .

### 1.3.3 Applications of Polymers at Surfaces

In many natural and technical processes, the behavior of polymers near surfaces and interfaces plays an important role. This can be used in many medical and industrial

applications. For example, one can prevent the adsorption of bare particles from solution by grafting polymers onto a surface. This can be used in medical glassware that is inserted in a body for a prolonged period, for instance catheters. A bare glass surface is vulnerable for adsorption of bacteria [60]. After a period of time the result of such bacteria adsorption and subsequent multiplication can be an infection. Grafting polymers may prevent adsorption of bacteria on the glass, and therefore reduce the risk of an infection during a prolonged period of insertion.

In a similar way, liposomes, which are small containers made up of surfactant molecules in which a drug can be placed, can be coated by end-grafted polymers. When inserted in the blood stream the liposomes eventually adsorb on the surface of arteries, change their conformation and release the encapsulated drugs. The grafting of water-soluble polymers to the liposome surface can increase the period of circulation in the blood stream significantly. The kinetics of drug release can thus be controlled via grafting polymers on the liposomes.

In industry, one can find different applications for polymers at surfaces, such as adhesion, in which adhesion strength is maximized with an intermediate surface density and high molecular weight which allows for interpenetration and entanglement with matrix chains.

Another example, is lubrication, which can be best achieved with short chains at very high packing density such that little energy dissipation occurs when contacting a sliding surface [20].

## 1.4 Analytic Theories of Polymers at Surfaces

The goal of theories of polymer adsorption is to develop predictive equations for the structure of the layers, to relate their physical properties to all the factors which affect

them, and to explain the behavior of these layers in different types of solvents.

Two groups of theories, commonly referred to as “scaling theories” and “mean-field theories”, are used in the literature to provide a description of the density profiles of the layer and of the polymer-induced forces between surfaces [69]. Mean field theories are subdivided into two main categories, asymptotic self-consistent mean-field theory and numerical self-consistent mean-field theory. In this section, we review the scaling and analytic mean field theories.

### 1.4.1 Scaling Theory

**I ) Adsorbed Homopolymer** As a precursor to studying end-tethered polymers, we briefly consider adsorbed homopolymer. The scaling theory [32, 52, 73–77] of homopolymer adsorption in good and  $\Theta$  solvents was developed by de Gennes [32, 74]. It is based on the concept of a correlation length,  $\xi_b$ , for semidilute polymer solutions [27], which describes the concentration fluctuations of polymer in the system. He assumed that  $D$ , the thickness of an isolated adsorbed polymer chain, satisfies [26]

$$a \ll D \ll \xi_b \quad , \quad (1.7)$$

where  $a$  is a lattice parameter of a Flory-Huggins lattice used to model the monomer size. Eq. (1.7) puts limits on the validity of the calculations. The first inequality represents a limit of weak-coupling between monomers and surface. In this weak-coupling limit, results are independent of the details of the model.

The adsorbed layer is divided into three regions:

1. The proximal regime  $x < a$ , very near to the surface where the adsorbed chains experience constraints on their configurations and their density distribution is very sensitive to the details of the monomer-surface interaction.

2. The central regime,  $D < x < \xi_b$ . Here, the density profile obeys a universal power law and becomes independent of  $\phi_b$ , the volume fraction in the bulk.

3. The distal regime,  $x > \xi_b$ . Here the density profile,  $\phi(x)$ , approaches the bulk  $\phi_b$  exponentially.

For the central regime, the theory uses ideas applicable to a bulk system. In the bulk,  $\xi_b$  scales with the volume fraction of the polymer,  $\phi_b$ , as

$$\frac{\xi_b}{a} \simeq \begin{cases} \phi_b^{-3/4} & \text{good solvent} \\ \phi_b^{-1} & \Theta \text{ solvent} \end{cases} \quad (1.8)$$

De Gennes generalized this for this inhomogeneous system, by assuming that there is a local  $\xi$ , and it scales with the local  $\phi$  as

$$\xi(x) \sim [\phi(x)]^{-3/4} \quad , \quad (1.9)$$

in good solvents. Next, he chose  $\xi(x) \propto x$ , which is the distance from wall, and this leads to

$$x \propto [\phi(x)]^{-3/4} \quad . \quad (1.10)$$

This implies that

$$\phi(x) \propto x^{-4/3} \quad , \quad (1.11)$$

which gives the density profile.

The adsorbed amount,  $\Gamma$ , is obtained by integrating  $(\phi(x) - \phi_b)$  over the distance from the surface. Furthermore, one can obtain expressions for the free energy and interfacial tension,  $\gamma$ . Assuming that a true equilibrium in the system is achieved, it is possible to have consistent scaling laws for density profiles of polymer near a surface. The structure for the adsorbed layer is nearly independent of the bulk concentration, and self-similar.

## II ) End-Tethered Polymer

In 1980, de Gennes modeled uncharged end-tethered polymers [30], see figure 1.1. He assumed that the polymer does not adsorb on the surface. The chains are immersed either in a pure (good) solvent or in a solution of the same polymer.

Using scaling laws constructed by Alexander [78], he studied the conformations and the concentration profiles for long, flexible homopolymer chains grafted at one end to a surface using “blob” model.

The definition of a blob is a string of monomers which are unperturbed by intermolecular interactions. Successive blobs are considered as hard spheres [27].

In this theory, the diameter of the blobs is equated with the average distance between anchored polymers,  $d$ . He introduced a dimensionless measure of the number of chains per unit area as

$$\sigma = \left(\frac{b}{d}\right)^2 \quad (1.12)$$

For the brush limit and for a good solvent, the thickness,  $h$ , of the grafted layer, often called brush height, is given by

$$h \propto Zb\sigma^{1/3} \quad (1.13)$$

It depends on the number of chains grafted per unit area as well as on the molecular weight.

In this regime of stretched chains, the concentration profile is essentially flat, except for two adjustment regions at the ends. This implies that the chains are uniformly stretched and their ends are located at the edge of the brush. This assumption of the well-defined homogeneity of the brush layer, namely all chains in the brush are equally stretched with their terminals located at a distance,  $h$ , from the grafting surface, is a major simplification [28].

The surface pressure  $\pi$  of the brush depends on the number of blobs per unit area. The Alexander and de Gennes (ADG) model takes into account the correlations of the monomers inside the blob, which leads to

$$\pi \propto Z\sigma^{11/6} \quad (1.14)$$

To summarize, scaling theory predicts two regimes for end-grafted chains in good solvents, one unstretched and one stretched, depending on the average area per tethered chain,  $\Sigma$ . In both regimes a depletion layer near the wall has been predicted, although each chain must reach the grafted surface. At high coverage,  $\pi \propto Z\sigma^{11/6}$ .

## 1.4.2 Mean Field Theories

### I ) Adsorbed Homopolymer

In mean field theory, all instantaneous intermolecular interactions are replaced by time average interactions. Mean field theories of polymers do not include fluctuations in the total density, but can include chain fluctuations.

The mean-field models can be analytical or numerical [69]. They are based on the earlier works by Edwards [79].

A key element of most mean field theories is the probability distribution function which describes the probability that a polymer of length  $\tau$  ends at  $\mathbf{r}'$  if it begins at  $\mathbf{r}$ . This function obeys a modified diffusion equation, which can be solved in terms of eigenfunctions and eigenvalues. In the ground state dominance approximation, only the lowest eigenvalue and eigenstate are retained in the solution.

Edwards and Dolan [80] applied the mean-field theory to the interactions between surfaces bearing polymer chains [69]. Jones and Richmond [110] studied adsorption from good and  $\Theta$  solvents onto a planar surface, using the self-consistent field theory (SCF) of Edwards and Dolan. Their procedure is based on the ground state

dominance approximation for the solution of a diffusion equation.

Semenov *et al.* [51, 81] went beyond the ground-state-dominance approximation, and introduced the so-called two-order-parameter theory. These order parameters describe the monomer and the chain end distributions. The theory can be used to estimate the forces between two polymer layers in full equilibrium with a bulk solution, as has been done by Bonet-Avalos *et al.* [82].

The mean-field theories can predict qualitative information on the structure and physical properties of the adsorbed layer, in addition to describing forces among components of the system at conditions where steric interactions dominate (at high surface concentrations). On the other hand, at conditions where bridging interactions become important (at low coverages), the mean-field theories fail to predict the bridging attraction between the surfaces [69].

## II ) End-Tethered Polymer

By the end of 1980's, the brush had been treated theoretically by analytical (asymptotic) self-consistent field theory (aSCF). This model has been developed independently and simultaneously by Milner, Witten and Cates (MWC) [41, 87], and Zhulina, Borisov, Priamitsyn and Birshtein [88].

In the aSCF model, it is assumed that the grafting density of the brush is sufficiently high to make the grafted layer laterally homogeneous. Consequently, the monomer density is solely a function of the distance from the grafting surface. The key point of the aSCF theory is based on an analogy between the configuration of the polymer chains and the trajectories of a classical particle moving in a harmonic potential. In this analogy, the monomer number  $\tau$  corresponds to the time  $\tau$  of the moving particle. The grafted chain with  $Z$  segments requires  $Z$  "timesteps" to reach the surface, irrespective of where it starts.

In the mechanical analogue, the chain path,  $x(\tau)$ , becomes the particle trajectory.

The particle reaches the surface in a “time”  $\tau$  that is independent of its starting point. This “equal time” potential is therefore harmonic.

In the aSCF theory for good solvent conditions, only binary interactions between polymer segments are taken into account [64]. Because the general form of an equal-time potential field is quadratic, and for low polymer density the effective potential in the aSCF model is proportional to the monomer density, it follows that the composition profile of the polymer density is parabolic in good solvent. It then follows that the brush scales the same way as in scaling theory,  $h \sim Z\sigma^{1/3}$ .

However, there is a slight difference between the aSCF prediction for surface pressure of the brush, which scales as

$$\pi \propto Z\sigma^{5/3} \quad , \quad (1.15)$$

and the ADG scaling theory Eq. (1.14).

It must be noted that these results should apply to the limits of high molecular weight  $Z$ , and moderately high surface coverage,  $\sigma^*$ , and weak excluded-volume interactions. The aSCF procedure neglects the polymer depletion layer near the surface and the existence of the smooth, stretched tails of the layer ends.

As seen above, both the MWC model and the ADG model give the same scaling relationships for the thickness of the brush, but they predict different numerical prefactors. However, the power law exponents of  $\pi$  as a function of  $\sigma$  differ slightly. Moreover, they predict different shape profiles.

It should be clarified that aSCF model does have some defects. The most serious one is its assumption that all the chains are in their most probable conformation: no fluctuations around this conformation are considered. In a particular case, the aSCF formalism neglects the interpenetration of brushes on opposing surfaces. This predicted picture of compression is another approximation.

### 1.4.3 Diblock Copolymer Adsorption

The discussions in the previous sections for homopolymer adsorption and the brush regime can be used to describe the adsorption of diblock copolymers.

Mean-field and scaling predictions of diblock copolymer adsorption from selective and nonselective solvents were originally suggested by Marques *et al.*[36, 64]. In the first step, they studied the adsorption of an  $A$ – $B$  diblock copolymer from a dilute solution onto a solid surface in a nonselective solvent. The solvent was considered to be good for the two incompatible blocks.

The solid surface was assumed to interact differently with each block. It strongly attracts the  $A$  block and strongly repels the other block. When thermodynamic equilibrium is achieved and for a dilute solution, the structure of the adsorbed layer is specified essentially by the asymmetry of the copolymer.

For non-selective solvents the asymmetry parameter is the ratio

$$\beta = \frac{R_B}{R_A} = \left( \frac{Z_B}{Z_A} \right)^\nu . \quad (1.16)$$

Where they used  $\nu = \frac{1}{2}$  and  $\frac{3}{5}$  for mean field and scaling theories respectively. While  $R_A$  and  $R_B$  are the radii of gyration of adsorbed and buoy block, respectively. In the mean-field theory, the radii of gyration are

$$R_A = Z_A^{1/2}b, \quad R_B = Z_B^{1/2}b \quad , \quad (1.17)$$

where  $Z_A$  and  $Z_B$  are the degrees of polymerization of  $A$  and  $B$  blocks, respectively, and  $b$  is the statistical segment length, which is assumed to be the same for both blocks. In this model it has been always assumed that  $\beta \gg 1$ . They studied two limits depending on the parameter,  $\beta$ .

The first is  $\beta < Z_A^{1/2}$ . Here, they found that the anchored layer in contact with the surface is a continuous “fluffy” layer, in which the density profile decays in a

way similar to adsorbed homopolymer layer. However, the existence of the dangling block in the solution reduces the number of adsorbed  $A$  blocks, and prevents this layer from reaching the same equilibrium surface coverage as a corresponding homopolymer layer. This results in the thickness of the adsorbed layer being smaller for block copolymers than for homopolymers. The dangling block,  $B$ , forms a brush layer with height,  $h$ , scaling linearly with molecular weight.

The second regime occurs when the nonadsorbing block is much larger than the adsorbing one, i.e,  $\beta > Z_A^{1/2}$ . Then, the anchored  $A$  block breaks into individual chains forming a discontinuous flat “pancake” on the surface and this anchored layer has a thickness on the order of monomer size  $a$ , forming a quasi-two-dimensional polymer solution which is either dilute or semidilute.

In a highly selective solvent the adsorbed  $A$  block is in a poor environment. This forces it to collapse onto the surface to make a molten layer on the solid wall, where the solvent does not penetrate into the layer. The  $B$  block is in a good solvent, which causes it dangle into the solution and form a brush attached to the molten layer. The physical structure of the adsorbed layer is predicted by the chemical potential of the dangling block in solution.

The dominant interaction in this case is the van der Waals interaction between the surface and the molten  $A$  layer. The asymmetry between the two parts of the copolymer is measured by

$$\beta = \frac{Z_B^{3/5}}{Z_A^{1/2}} \quad , \quad (1.18)$$

which drives the formation of the molten layer. If this ratio is large enough, the thickness of the molten layer results from a balance between the van der Waals energy and the stretching energy of the brush.

## 1.5 Experimental Studies of End-Tethered Polymers

The physical properties and structure of the air-liquid interface of polymer solutions with good and  $\Theta$  solvents have been examined extensively experimentally. For example, the adsorption from solution of polydimethylsiloxane (PDMS) homopolymer in good (bromoheptane) and  $\Theta$  (bromocyclohexane) solvents was investigated by Kent *et al.* [7]. Using x-ray evanescent wave induced fluorescence (XEWIF), the effects of molecular weight, bulk concentrations and solvent quality on the adsorbed profiles of the polymer near the interface were probed.

They found the adsorbed amount in dilute solution for near  $\Theta$  conditions is about four times larger than in a good solvent, with the profile decaying much more slowly with depth than in the case of good solvent.

In good solvent, and in dilute solution, they found that the region of the profile nearest to the surface ( $\sim 4$  nm) is roughly independent of molecular weight, in agreement with theoretical predictions. On the other hand, for the near- $\Theta$  conditions, and for dilute solution, they found that there is a stronger dependence of the adsorbed amount on the molecular weight for the region of the profile within ( $\sim 4$  nm) of the surface [7].

In another study of the surface tension of polymer solutions, Ober *et al.* [108], explored the adsorption from solution of poly(dimethylsiloxane) PDMS in toluene and polystyrene (PS) in toluene for attractive and repulsive surfaces, respectively. Toluene is a good solvent for both polymers. They found that PS adsorbs at the free surface and a concentration excess appears there, while the density of PDMS at the surface was lower than in the bulk.

Various techniques have been used to study layers of tethered polymers. An

important one is the surface force measurements on layers of adsorbed copolymers by Hadziioannou *et al.* [95], Israelachvili *et al.* [2], Patel *et al.* [96], Marra *et al.* [97], and Taunton *et al.* [98]. The first measurements focused on studying the long range forces between layers of adsorbed copolymers, and on probing the relation between these forces and the thicknesses. The analysis of these experiments was done using the aSCF theory and scaling theory. Subsequent experimental work includes small-angle neutron-scattering (SANS) [4, 6, 100], and neutron reflectivity measurements [3, 5, 8, 101].

Auroy [4] used small-angle neutron-scattering to determine the scaling behavior of polydimethylsiloxane chains tethered to porous silica. They examined two categories of solvents: bad solvents, in which they observed  $h \sim Z\sigma$ , and good solvents in which they found  $h \sim Z\sigma^{1/3}$ . These results provided the first experimental evidence of the brush limit.

Field *et al.* [9] used neutron reflectometry to measure the density profile of four PS-PEO copolymers adsorbed on quartz from deuterated toluene. The density profiles of the dangling PS could be well-described by a parabolic or error function with maximum at the surface and an exponential-like tail.

Two sets of results for good solvent cases are of particular importance to this thesis, one by Kent *et al.* [8, 12, 102] and the other by Bijsterbosch *et al.* [11].

The system studied by Kent *et al.* is shown in Figure 1.2. They used poly(dimethylsiloxane)-polystyrene (PDMS-PS) diblock copolymers with ethyl benzoate as the solvent. In this case, the PS-block is the dangling block and the PDMS-block anchors the polymer to the air-liquid surface. In these experiments, both molecular weight and surface coverages were varied independently, each over an order of magnitude.

They reported that in these experiments the maximum attainable surface coverages were limited by a sharp rise in surface pressure, so  $\sigma^*$  varied from about 1 to

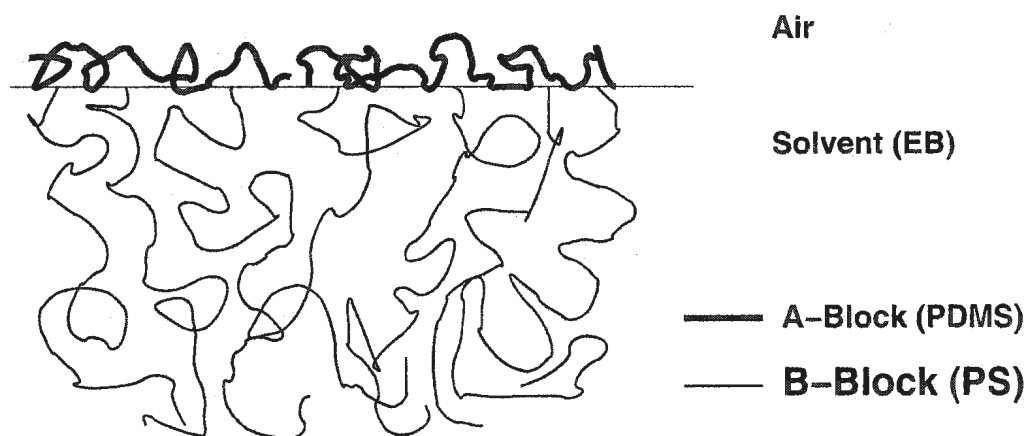


Figure 1.2: Illustration of the monolayer system formed by PDMS-PS diblock copolymer on EB

12. This means that, in these and other experiments on layers formed from polymers in dilute solution, the maximum value for the reduced surface concentration,  $\sigma^*$ , is about 12. They also concluded that the thickness of the tethered layer does not scale as  $Z\sigma^{1/3}$  as predicted by (aSCF) model and de Gennes scaling theory. Instead, they found that it scales approximately as  $Z^{0.86}\sigma^{0.22}$  [12].

Polymer chains adsorbed at the surface reduce the surface tension. This change can be interpreted as the two-dimensional pressure,  $\pi$ . Kent *et al.* measured  $\pi$ , and then subtracted the contribution due to the adsorbed block, thereby extracting the excess surface pressure due to the dangling block,  $\Delta\pi$ . This procedure is discussed in chapter 3. They found that  $\Delta\pi$  as a function of coverage increases up to a certain threshold but, beyond that,  $\Delta\pi$  increases sharply, much more rapidly than predicted by scaling and aSCF theories. However, it is still approximately a power law. The value of exponent ranges from approximately 4.2 to 6.6, and increases slightly with  $Z$ . These values are much larger than the values of 11/6 or 5/3 predicted by scaling and aSCF theories.

Bijsterbosch *et al.* [11] used neutron reflectivity to study a series of polystyrene

-poly-(ethylene oxide) (PS-PEO) diblock copolymers in water, with varying lengths of the PEO-block. In this system, the PS anchors to the air-water interface, and the PEO dangles into the water which is a good solvent. They reported three regions for surface pressure. The first is at low surface density, where the pressure is very low and is due to intermolecular interactions. The second is at intermediate coverage, where the PEO block gradually desorbs to form a brush, and the pressure increases. Finally, it begins to increase again at coverage where the brush is laterally compressed. Currie *et al.* [60] subsequently showed that these results in this third region are compatible with aSCF theory with  $\Delta\pi \sim \sigma^{5/3}$ . In their experiments Bijsterbosch *et al.* reached high reduced surface coverages, up to  $\sigma^* \lesssim 27$ . This contrasts with the upper limit of  $\sigma^* \simeq 12$  for end-grafted layers formed from polymers in dilute solution, obtained by Kent's experiments.

More details on the results obtained by Kent *et al.* and Bijsterbosch *et al.* will be presented in chapter 3, taking into account the results calculated using (nSCF) theory done in this thesis.

## 1.6 Numerical Models

The experimental results just discussed suggest that numerical calculations are needed for quantitative agreement. Grest [49] carried out molecular dynamics simulations of 4 chain lengths in good and  $\Theta$  solvents, with  $Z$  ranging from 25 to 200 and surface concentration of  $\sigma^* \lesssim 20$ . His results for the dependence of the surface pressure on the grafting density were somewhat stronger than predicted by scaling theories. For a good solvent, and for high surface coverage of tethered chains which were strongly stretched, Grest concluded that the height of the brush  $h$ , was in reasonable agreement with a scaling of  $h \propto Z\sigma^{1/3}$ , while the surface pressure scaled as  $\pi \propto \sigma^{2.5}$ . Baranowski

and Whitmore [39] subsequently showed that the height of the brush in Grest's work shows a weaker molecular weight dependence than he originally concluded.

Numerical self-consistent field (nSCF) theory incorporates finite molecular weight effects [38, 47, 50, 91, 92]. The first nSCF theories used Scheutjens and Fler's lattice mean-field theory [34, 83, 84] and its variations [85]. Scheutjens and Fler originally studied simple homopolymer adsorption using first-order Markov chain statistics [34, 83, 84]. Van der Linder *et al.* [86] extended the pioneering theory of Scheutjens and Fler to semi-flexible polymers, taking into account bond correlations.

Studies have been performed using nSCF theory to investigate the behavior of tethered layers in good solvents under non-adsorbing conditions. The results of the layer thickness generally differ from those obtained by aSCF theory, i.e.,  $h \sim Z\sigma^{1/3}$ . In one study using this model in addition to Monte Carlo calculations [111], fitting to the sets of results gave

$$h_{rms} \propto Z^\nu \sigma^\mu \quad , \quad (1.19)$$

where  $\nu = 0.86$  and  $\mu = 0.27$ , consistent with previous work performed using the same model [39] in which  $\nu = 0.81$  and  $\mu = 0.24$ . These results agree well with Kent's experiments.

Carignano and Szleifer [47], applied single-chain mean-field theory to study the behavior of a mobile and tethered chain in different solvent qualities. They performed numerical calculations to examine the pressure isotherms in good and  $\Theta$  solvents, for chains of  $Z = 50$  and surface coverages up to  $\sigma^* = 40$ , obtaining very good quantitative agreement with results of the MD simulations of Grest [49]. They found that the lateral pressure for good solvent for very low surface coverage ( $\sigma^* \ll 1$ ), can be described approximately by a power law with exponent equal to 2. On the other hand, for intermediate surface coverage up to  $\sigma^* \lesssim 18$  the exponent is 1.9, whereas

$\pi \propto \sigma^{2.1}$  for surface coverage  $19 \lesssim \sigma^* \lesssim 40$ . Comparisons with the aSCF model showed good agreement only when the parabolic density profile is used in the full virial equation, and only for the intermediate and high surface coverage regimes.

In their later study, [50] Carignano and Szleifer investigated another 4 chain lengths with  $Z$  ranging from 30 to 100 and surface coverages of  $\sigma^* \lesssim 20$ . Their predictions for both the brush height and lateral surface pressure as a function of surface coverage were compared to the results obtained by Kent *et al.* [12]. They found excellent agreement for the height of the brush for all surface coverages, since their results scaled as  $h \sim Z^{9/10} \sigma^{1/4}$ , which is consistent with the nSCF predictions. They showed that the experimental lateral pressures multiplied by the square of the bulk radius of gyration, i.e.  $\Delta\pi R_g^2$ , is a universal function of the reduced surface coverage,  $\sigma^*$ . They reported that  $\Delta\pi$  is in good agreement with the experimental results of Kent *et al.* up to  $\sigma^* \sim 8$ . For higher reduced surface coverages their theoretical results deviate from what had been found by the experiments. They attributed this deviation to non-equilibrium conditions in the experiments. However, in Kent's experiments, it is found that the rapid rise in surface pressure occurs for different values of  $\sigma^*$ . For example, for 4-30 PDMS-PS copolymer it occurs at  $\sigma^* \sim 4$ , while for 28-330 PDMS-PS and 4.5-60 PDMS-PS copolymers it occurs at  $\sigma^* \sim 7$ .

An important set of calculations for work in this thesis is one done by Baranowski [72]. He used nSCF calculations, and found a rapid increase in excess pressure, in semi-quantitative agreement with experiments of Kent *et al.* but in disagreement with all other theories and with the Bijsterbosch experiments. Fig. 1.3 shows the behavior of the surface pressure excess as a function of the number of chains per unit area for the 28-330 PDMS-PS copolymer as calculated by Baranowski [72]. It shows two distinct regimes. In the first one,  $\Delta\pi$  can be described approximately by the power law dependence predicted by aSCF theory i.e.,  $5/3$ . On the other hand, in

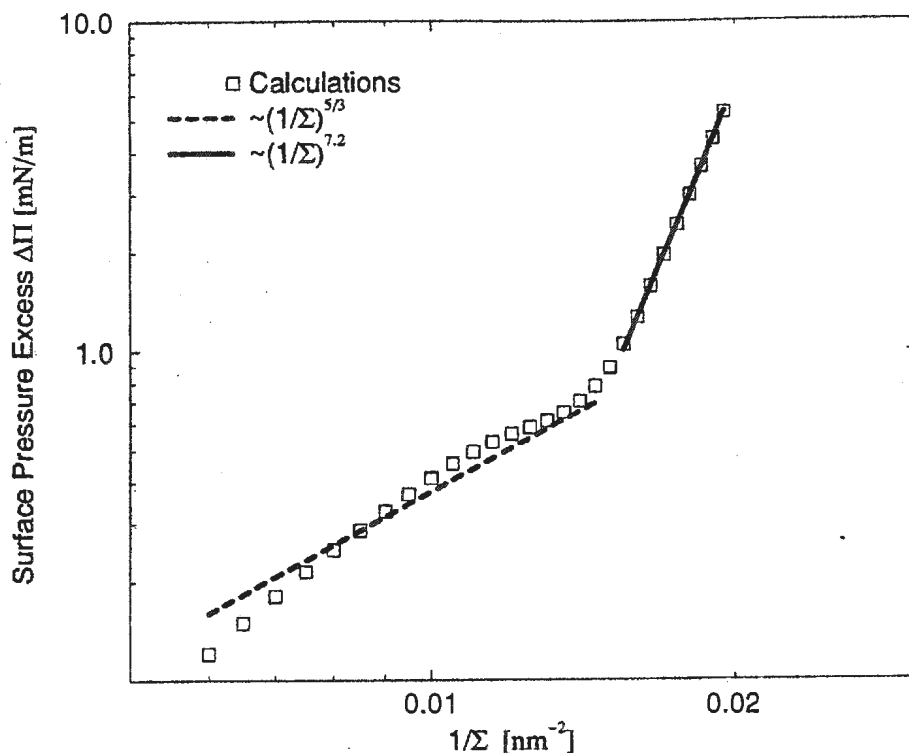


Figure 1.3: Two regimes for surface pressure excess,  $\Delta\pi$  as a function of the number of chains per unit area for the 28-330 PDMS-PS copolymer. The solid line is fitted to the calculations done by Baranowski. While the dashed line is the line of the best fit of  $5/3$  power law dependence.

the second regime a sudden sharp rise is noted, still described by a power law, but with an exponent of 7.2. However, Currie *et al.* [60], used the Scheutjens-Fleer nSCF model to model the experiments carried out by Bijsterbosch *et al.* [11]. They found semi-quantitative agreement with the experiments and with the aSCF predictions,  $\pi \sim \sigma^{5/3}$  and  $h \sim \sigma^{1/3}$ , with surface pressure and thickness depend on density.

The case of a PEO-block with 700 monomers is an illustrative example, Currie *et al.* [60], found that the surface pressure isotherms when plotted on a double logarithmic plot, had some interesting features. For a good ( $\chi = 0$ ) and a  $\Theta$  solvent

( $\chi = 1/2$ ), where  $\chi$  is known as the Flory-Huggins interaction parameter, and taking into account that  $\chi_{surface}$ , which is the interaction of homopolymer or one block of copolymer with the surface, is set zero for both solvent qualities, the isotherm showed, at low densities, that the surface pressure is proportional linearly to the grafting density, and is independent of the solvent quality. This indicates that the system under these conditions exhibits an ideal gas behavior for non-interacting coils. This contrasts with the result found by Carignano and Szleifer [47], in which they showed a quadratic dependence of the surface pressure on the grafting density at very low densities. Currie *et al.* claimed that this unrealistic physical result arose from the incorrect expression for the surface pressure used by Carignano and Szleifer [47]. At higher coverages, Currie *et al.* found the power law exponent to be very close to  $5/3$ , as predicted by the aSCF theory, and in contrast with Baranowski's result of a second region.

## 1.7 Objective and Outline of this Work

The goals of this thesis are to re-examine Baranowski's calculations [72] and confirm his results. What is the behavior of the excess surface pressure,  $\Delta\pi$ , as a function of density? Does nSCF theory produce the results observed by Kent *et al.*, and calculated by Baranowski as shown in Fig. 1.3, or those observed by Bijsterbosch *et al.*, and all other theories? In order to address these questions, we use the following procedure.

All the important system parameters that are needed are known best for the system studied by Kent *et al.*, namely PDMS-PS in EB. Used in nSCF theory, they gave excellent agreement for the density profiles and layer thicknesses. For these reasons, we focus on this system and use nSCF theory.

We first model the homopolymer PDMS/EB system with an attractive surface interaction, and calculate, using nSCF theory, the surface pressure as a function of coverage. Then, we model PDMS-PS/EB system, and calculate the surface pressure. The excess surface pressure,  $\Delta\pi$ , is then calculated as the difference between the surface pressure for the diblock copolymer system and the system when only the homopolymer exists. In carrying out all these calculations, the author used Baranowski's computer code to model systems under investigation. As will be described later, there are two approximations that were examined in order to probe the difference between Baranowski's results [72] and results obtained in this thesis. These approximations are reflected in two parameters, which are described in section 3.2.5.

Then we compare the results obtained by nSCF calculations for the Kent *et al* experiments with the experimental results reported by Bijsterbosch *et al.*, which have been modeled using nSCF theory by Currie *et al.* [60].

# Chapter 2

## Numerical Self-Consistent Field Theory

### 2.1 Introductory Remarks

Real systems comprised of a large number of polymer macromolecules and solvent molecules interacting with each other can be well-understood using numerical approaches. Generally speaking, the description of the system can be determined as the following:

1. Specification of the various microscopic configurations of the system which correspond to the macroscopic state, and for each configuration, calculation of its energy.
2. Evaluation of the configurational part of the partition function  $\mathcal{Z}$ .
3. Determination of the Helmholtz free energy

$$\mathcal{F} = -k_B T \ln \mathcal{Z} \quad . \quad (2.1)$$

Once the free energy is calculated, other physical quantities can be determined.

Polymer configurations can be modeled as walks in continuous space or as walks on a discrete lattice. The first choice leads to a continuous (nSCF) theory. The second choice leads to a lattice model, which is represented by Scheutjens and Fleer theory [34, 83, 84]. Each step in the walk is determined with two factors, a local entropy of mixing and an energy factor describing the short-range interactions with the nearest neighbors. The lattice sites are filled by either monomer or a solvent molecule. A set of self-consistent equations is derived and solutions have to be found numerically.

The nSCF theory based on continuous space curve representation of the polymers is presented here. The formalism is based on the SCF theory introduced by Edwards and Dolan [79, 80] and further developed by Hong and Noolandi [31], Helfand *et al.*, [103], Ohta and Kawasaki [104], Whitmore and Noolandi [40, 43], and Banaszak [105]. In order to give a full statistical description for polymer/solvent systems, one needs to describe the various microscopic configurations of the system. In doing so, one needs to first specify models for linear flexible polymer chains and their interactions. These interactions are divided into kinds:

1. The energy explicitly due to the sequence of bonds along the chains. It includes local chain connectivity constraints, trans-gauche bond sequence energies, etc. This energy can be conceptualized as that required to put the monomers down sequentially. This is called the "short range interactions". They are related to the structural characteristics of the macromolecule, considering bond types and the interactions between segments or neighboring atoms. These factors originate from steric repulsions, which limit the values of the internal angles of rotation of the bonds within the chain. Hence, the random coil will expand, in order to avoid such repulsions.

2. Energy due to interactions between monomers which are far separated along a chain, but near to each other in space. This includes all other contributions to the energy. This type is called "long range interactions".

The long range interactions are mediated by the solvent, creating effective monomer-monomer interactions. These effective interactions vanish at the  $\Theta$  point, and the chains become ‘ideal polymers’ [106].

We can also define the  $\Theta$  point using the osmotic pressure. Consider a dilute solution of polymers in solvent. A dilute solution is defined as one in which the polymer concentration is small enough that the average distance between molecules is greater than the size of a molecule. Now, let  $F_M$  denote the free energy of mixing of the polymer and solvent. Then the osmotic pressure is defined as

$$\Pi_{osmotic} = - \left( \frac{\partial F_M}{\partial V} \right)_{T,p,n_p}, \quad (2.2)$$

where  $n_p$ ,  $p$  and  $T$  are the number of polymer molecules, external pressure and temperature, respectively. The osmotic pressure can be expressed also in the form of a virial expression

$$\Pi_{osmotic} = N_A k_B T c_p \left( A_1 + A_2 c_p + A_3 c_p^2 + \dots \right), \quad (2.3)$$

where  $N_A$  is the Avogadro’s number,  $c_p$  is the polymer concentration and the  $A_i$  are the virial coefficients [27]. Equation (2.3) has the same form as the virial expansion for a gas.  $A_2$  is called the second virial coefficient. It has the form

$$A_2 \propto \left( 1 - \frac{\Theta}{T} \right). \quad (2.4)$$

In good solvent,  $A_2 > 0$ . However, at temperature  $T = \Theta$ ,  $A_2 = 0$ , and the dilute solution acts as an ideal gas of point particles. This temperature,  $\Theta$ , is called  $\Theta$  temperature.

One of the important quantities that describe polymer chain is the probability distribution function for the end-to-end vectors. A polymer in a  $\Theta$  solvent is ideal, and the distribution function for each bond can be modeled as a Gaussian distribution,

defined as

$$\psi(\mathbf{r}) = \left( \frac{3}{2\pi b^2} \right)^{3/2} \exp \left( -\frac{3\mathbf{r}^2}{2b^2} \right) , \quad (2.5)$$

where  $b$  is the effective bond length referred to as the statistical segment length, and  $\mathbf{r}$  is the bond vector.

## 2.2 Partition Function

In this section, we introduce the general theory for the diblock copolymer spread as a monolayer at the air-liquid interface. The system which we are dealing with can be described by  $\tilde{N}_C$  diblock copolymer chains and  $\tilde{N}_S$  solvent molecules in some volume  $V$ .

A diblock copolymer consists of  $A$  and  $B$  blocks. Block  $A$  is characterized by its degree of polymerization,  $Z_A$ , effective bond length,  $b_A$ , and the number density of pure material,  $\rho_{oA}$ , in monomers per unit volume. Similarly, block  $B$  can be specified by  $Z_B$ ,  $b_B$ , and  $\rho_{oB}$ . For solvent molecules, the density of pure material,  $\rho_{oS}$ , has to be specified. Since the system consists of  $\tilde{N}_C$  chains, the total number of monomers of type  $\kappa$  is  $N_\kappa = \tilde{N}_C Z_\kappa$ ,  $\kappa = A, B$ .

At this point it is useful to introduce the incompressibility condition [31] which ensures conservation of volume on mixing. This condition is equivalent to the local volume fractions adding up to unity everywhere

$$\sum_{\kappa} \frac{\langle \hat{\rho}_\kappa(\mathbf{r}) \rangle}{\rho_{o\kappa}} = 1, \quad \kappa = A, B, S , \quad (2.6)$$

where  $\hat{\rho}_\kappa(\mathbf{r})$  is the local number density of species  $\kappa$  for a given configuration, and  $\langle \dots \rangle$  denotes the ensemble average.

Assuming there is no volume change upon mixing, the configurational partition function can be written using functional integrals over all possible chain configurations

and locations of solvent molecules

$$\begin{aligned}
Z = & \left( \prod_{\kappa=C,S} \frac{\mathcal{Z}_\kappa^{\tilde{N}_\kappa}}{\tilde{N}_\kappa!} \right) \int \left( \prod_{i=1}^{\tilde{N}_S} d\mathbf{r}_{Si} \right) \times \\
& \int \prod_j^{\tilde{N}_c} \delta \mathbf{r}_{Aj}(\cdot) P[\mathbf{r}_{Aj}(\cdot)] \mathcal{G}(\mathbf{r}_{Aj}(0)) \delta \mathbf{r}_{Bj}(\cdot) P[\mathbf{r}_{Bj}(\cdot)] \times \\
& \delta(\mathbf{r}_{Bj}(Z_B) - \mathbf{r}_{Aj}(Z_A)) \times \\
& \prod_{\mathbf{r}} \delta \left( 1 - \sum_{\kappa=A,B,S} \frac{\hat{\rho}_\kappa(\mathbf{r})}{\rho_{o\kappa}} \right) \times \\
& \exp[-\beta \hat{V}] .
\end{aligned} \tag{2.7}$$

In this expression  $P[\mathbf{r}_{\kappa j}(\cdot)]$  represents the Wiener measure for a chain with configuration  $\mathbf{r}_{\kappa j}(\cdot)$ ,  $\delta \mathbf{r}_{\kappa j}(\cdot)$  denotes the integration over all possible chosen configurations, and the kinetic energy contribution of a solvent molecule or polymer chain is denoted by  $\mathcal{Z}_\kappa$ . The function  $\mathcal{G}(\mathbf{r}_{Aj}(0))$  is introduced here for convenience. It describes the a priori probability distribution for the free end of an  $A$  type chain. In most cases, it is simply  $\mathcal{G} = 1$  everywhere. However, in those cases where, for physical reasons, the chain is localized to a particular interfacial region, it is convenient to use  $\mathcal{G}(\mathbf{r}_{Aj}(0))$  in the form

$$\begin{aligned}
\mathcal{G}(\mathbf{r}_{Aj}(0)) &= 0 & \text{if } \mathbf{r}_j(0) \notin \text{interface} \\
0 < \mathcal{G}(\mathbf{r}_{Aj}(0)) &\leq 1 & \text{if } \mathbf{r}_j(0) \in \text{interface} .
\end{aligned} \tag{2.8}$$

Thus from all possible conformations of chains, only these which have the  $A$  type end of every chain in the interface contribute. This explicit form is used only in the calculations of chapter 3 of this thesis.  $\delta(\mathbf{r}_{Bj}(Z_B) - \mathbf{r}_{Aj}(Z_A))$  ensures that one end of each of the two blocks of each copolymer chain occupies the same point in space, i.e., that they are bonded together at the joint [40]. The condition of incompressibility is imposed by the delta expression  $\delta \left( 1 - \sum_{\kappa} \frac{\hat{\rho}_\kappa(\mathbf{r})}{\rho_{o\kappa}} \right)$  [104].

The potential  $\beta \hat{V}$  which appears in Eq. (2.6) is due to the long-range interactions between all components present in the system and interactions with the boundaries.

It is a function of the microscopic particle densities which are modeled as

$$\hat{\rho}_S(\mathbf{r}) = \sum_{i=1}^{\tilde{N}_S} \delta(\mathbf{r} - \mathbf{r}_{Si}) \quad , \quad (2.9)$$

$$\hat{\rho}_\kappa(\mathbf{r}) = \sum_{j=1}^{\tilde{N}_C} \int_0^{Z_\kappa} d\tau \delta(\mathbf{r} - \mathbf{r}_{\kappa j}(\tau)) \quad , \quad (2.10)$$

where  $\mathbf{r}_{\kappa j}(\tau)$  describes the position of monomer  $\tau$  of type  $\kappa$  in  $j$  chain.

As in most polymer theories, it is assumed that binary interactions are sufficient to describe real polymers in a solution [64]. The interaction potential energy can be written

$$\begin{aligned} \beta \hat{V} \equiv \hat{W} &= \frac{1}{2} \sum_{\kappa \kappa' = A, B, S} \int d\mathbf{r} \int d\mathbf{r}' \hat{\rho}_\kappa(\mathbf{r}) W_{\kappa \kappa'}(\mathbf{r} - \mathbf{r}') \hat{\rho}_{\kappa'}(\mathbf{r}') + \\ &\quad \sum_{\kappa = A, B, S} \int d\mathbf{r} \hat{\rho}_\kappa(\mathbf{r}) u_\kappa(\mathbf{r}) \quad , \end{aligned} \quad (2.11)$$

where  $W_{\kappa \kappa'}(\mathbf{r} - \mathbf{r}')$  defines the potential acting on a particle of type  $\kappa$  at the position  $\mathbf{r}$  due to a particle of type  $\kappa'$  at the position  $\mathbf{r}'$ , and  $u_\kappa(\mathbf{r})$  is the potential experienced by component  $\kappa$  due to the surface.

Equations (2.9) and (2.10) express the microscopic densities in terms of the individual solvent molecules and chain segments. Since the polymer chains are modeled by continuous chains, it is essential to convert the microscopic densities to continuous functions. This can be done through the introduction, for each independent function  $\hat{\rho}_\kappa(\mathbf{r})$ , of a Dirac delta function

$$\begin{aligned} \prod_{\mathbf{r}} \delta \left( 1 - \sum_{\kappa = A, B, S} \frac{\hat{\rho}_\kappa(\mathbf{r})}{\rho_{o\kappa}} \right) \exp[-\hat{W}] &= \\ \int \left\{ \prod_{\kappa = A, B, S} \delta \rho_\kappa(\cdot) \delta[\rho_\kappa(\cdot) - \hat{\rho}_\kappa(\cdot)] \right\} \prod_{\mathbf{r}} \delta \left( 1 - \sum_{\kappa = A, B, S} \frac{\rho_\kappa(\mathbf{r})}{\rho_{o\kappa}} \right) \exp[-W(\{\rho_\kappa(\cdot)\})] &, \end{aligned} \quad (2.12)$$

where  $W(\{\rho_\kappa(\cdot)\})$  is defined in Eq. (2.11) but for continuous  $\{\rho_\kappa(\mathbf{r})\}$ .

Using the Fourier transform for each Dirac delta function, in addition to the continuous functions  $\rho_\kappa(\cdot)$ , leads to the following form for the partition function [40,

105]

$$\begin{aligned}
Z = & \left( \prod_{\kappa=C,S} \frac{Z_{\kappa}^{\bar{N}_{\kappa}}}{\bar{N}_{\kappa}!} \right) \times \int \left[ \prod_{\kappa=A,B,S} [\delta\rho_{\kappa}(\cdot)\delta w_{\kappa}(\cdot)] \right] \delta\eta(\cdot) \times \\
& \left( \prod_{\kappa=C,S} Q_{\kappa}^{\bar{N}_{\kappa}} \right) \times \exp \left[ \int d\mathbf{r} \eta(\mathbf{r}) \left( 1 - \sum_{\kappa=A,B,S} \frac{\rho_{\kappa}(\mathbf{r})}{\rho_{0\kappa}} \right) \right] \times \\
& \exp \left[ \sum_{\kappa=A,B,S} \int d\mathbf{r} w_{\kappa}(\mathbf{r}) \rho_{\kappa}(\mathbf{r}) \right] \times \exp[-W[\{\rho_{\kappa}(\cdot)\}]] \quad , \quad (2.13)
\end{aligned}$$

where  $\eta(\mathbf{r})$  is the Lagrange multiplier field arising from the incompressibility condition.

For solvent

$$Q_S = \int d\mathbf{r} \exp[-w_S(\mathbf{r})] \quad , \quad (2.14)$$

and for copolymer

$$\begin{aligned}
Q_C = & \int \delta\mathbf{r}_A(\cdot)\delta\mathbf{r}_B(\cdot)P[\mathbf{r}_A(\cdot)]P[\mathbf{r}_B(\cdot)]\mathcal{G}(\mathbf{r}_A(0)) \times \\
& \exp \left[ - \int_0^{Z_A} d\tau w_A[\mathbf{r}(\tau)] \right] \exp \left[ - \int_0^{Z_B} d\tau w_B[\mathbf{r}(\tau)] \right] \times \\
& \delta(\mathbf{r}_B(Z_B) - \mathbf{r}_A(Z_A)) \quad . \quad (2.15)
\end{aligned}$$

One can introduce the propagators

$$\begin{aligned}
Q_{\kappa}(\mathbf{r}, \tau | \mathbf{r}', 0) = & \int \delta\mathbf{r}_{\kappa}(\cdot)\delta[\mathbf{r}_{\kappa}(\tau) - \mathbf{r}]\delta[\mathbf{r}_{\kappa}(0) - \mathbf{r}'] \times \\
& \exp \left\{ - \int_0^{\tau} d\tau' \left( \frac{3}{2b_{\kappa}^2} \left| \frac{d\mathbf{r}(\tau')}{d\tau'} \right|^2 + w_{\kappa}[\mathbf{r}_{\kappa}(\tau')] \right) \right\} \quad , \quad (2.16)
\end{aligned}$$

which satisfy the modified diffusion equation [106]

$$\left[ \frac{b_{\kappa}^2}{6} \nabla^2 - w_{\kappa}(\mathbf{r}) \right] Q_{\kappa}(\mathbf{r}, \tau | \mathbf{r}', 0) = \frac{\partial}{\partial \tau} Q_{\kappa}(\mathbf{r}, \tau | \mathbf{r}', 0) \quad , \quad (2.17)$$

with initial condition given by

$$Q_{\kappa}(\mathbf{r}, 0 | \mathbf{r}', 0) = \delta(\mathbf{r} - \mathbf{r}') \quad . \quad (2.18)$$

It turns out that the Green function  $Q_\kappa(\mathbf{r}, \tau | \mathbf{r}', 0)$ , represents the configurational partition function for one  $\kappa$  block of the chain starting at  $\mathbf{r}(0) = \mathbf{r}'$  and ending at  $\mathbf{r}(\tau) = \mathbf{r}$ .

The potentials  $w_\kappa(\mathbf{r})$  which modify the diffusion equations include enthalpic interactions between the molecules, written in terms of Flory parameters, plus a finite range correction which is of the order of a statistical segment length [31, 107], as well as interactions with the surface and terms arising from the incompressibility condition.

With these assumptions the integral of the distribution function, Eq. (2.15), can be written as

$$\mathcal{Q}_C = \int d\mathbf{r} d\mathbf{r}' d\mathbf{r}'' Q_B(\mathbf{r}, Z_B | \mathbf{r}', 0) Q_A(\mathbf{r}, Z_A | \mathbf{r}'', 0) \mathcal{G}(\mathbf{r}'(0)) \quad . \quad (2.19)$$

Finally, using the Stirling approximation, the partition function can be written as

$$Z = \mathcal{N} \int \prod_{\kappa=A,B,S} \delta\rho_\kappa(\cdot) \delta w_\kappa(\cdot) \delta\eta(\cdot) \exp[-\mathcal{F}_T[\{\rho_\kappa(\cdot)\}, \{w_\kappa(\cdot)\}, \eta(\cdot)]] \quad , \quad (2.20)$$

where  $\mathcal{F}_T[\{\rho_\kappa(\cdot)\}, \{w_\kappa(\cdot)\}, \eta(\cdot)]$  is the free energy functional (in units of  $k_B T$ ) given by

$$\mathcal{F}_T[\{\rho_\kappa(\cdot)\}, \{w_\kappa(\cdot)\}, \eta(\cdot)] = F[\{\rho_\kappa(\cdot)\}, \{w_\kappa(\cdot)\}] + G[\{\rho_\kappa(\cdot)\}, \eta(\cdot)] \quad , \quad (2.21)$$

with

$$F[\{\rho_\kappa(\cdot)\}, \{w_\kappa(\cdot)\}] = \left[ W[\{\rho_\kappa(\cdot)\}] - \sum_{\kappa=A,B,S} \int d\mathbf{r} w_\kappa(\mathbf{r}) \rho_\kappa(\mathbf{r}) \right] + \sum_{\kappa=C,S} \tilde{N}_\kappa \left\{ \ln \frac{\tilde{N}_\kappa}{Z_\kappa \mathcal{Q}_\kappa} - 1 \right\} \quad , \quad (2.22)$$

and

$$G[\{\rho_\kappa(\cdot)\}, \eta(\cdot)] = \int d\mathbf{r} \eta(\mathbf{r}) \left[ \sum_{\kappa=A,B,S} \frac{\rho_\kappa(\mathbf{r})}{\rho_{0\kappa}} - 1 \right] \quad . \quad (2.23)$$

## 2.3 The Saddle Function Method: Mean Field Approximation

The free energy of the system can be obtained by evaluating Eq. (2.20). However, this integration is too difficult to do completely. Instead, we use the saddle point method, keeping only those values of the fields that contribute most to the integral. This is equivalent to minimizing the free energy functional,  $\mathcal{F}_{\mathcal{T}}$ . Denote the corresponding values of the fields by  $\{\rho_{\kappa}^0(\mathbf{r})\}$ ,  $\{w_{\kappa}^0(\mathbf{r})\}$  and  $\eta^0(\mathbf{r})$ . The free energy, partition function and density distributions reduce to

$$\mathcal{F}_{\mathcal{T}} \rightarrow \mathcal{F}_{\mathcal{T}}[\{\rho_{\kappa}^0(\cdot)\}, \{w_{\kappa}^0(\cdot)\}, \eta^0(\cdot)] \quad , \quad (2.24)$$

$$Z \rightarrow Z^0 \propto \exp\{-\mathcal{F}_{\mathcal{T}}[\{\rho_{\kappa}^0(\cdot)\}, \{w_{\kappa}^0(\cdot)\}, \eta^0(\cdot)]\} \quad , \quad (2.25)$$

$$\langle \hat{\rho}_S(\mathbf{r}) \rangle \rightarrow - \left. \frac{\tilde{N}_S}{\mathcal{Q}_S} \frac{\delta \mathcal{Q}_S}{\delta w_S(\mathbf{r})} \right|_0 \quad , \quad (2.26)$$

$$\langle \hat{\rho}_{\kappa}(\mathbf{r}) \rangle \rightarrow - \left. \frac{\tilde{N}_C}{\mathcal{Q}_C} \frac{\delta \mathcal{Q}_C}{\delta w_{\kappa}(\mathbf{r})} \right|_0 \quad , \quad \kappa = A, B \quad , \quad (2.27)$$

where these last derivatives are evaluated at the minimum.

To find the saddle point,  $\mathcal{F}_{\mathcal{T}}$  has to be minimized with respect to each  $\rho_{\kappa}(\mathbf{r})$ ,  $w_{\kappa}(\mathbf{r})$  and  $\eta(\mathbf{r})$  subject to an additional constraint, namely that the total number of particles of each component in the system remains fixed:

$$\int d\mathbf{r} \langle \rho_{\kappa}(\mathbf{r}) \rangle = N_{\kappa} \quad \kappa = S, A, B \quad , \quad (2.28)$$

where  $N_S = \tilde{N}_S$ ,  $N_A = \tilde{N}_C Z_A$ , and  $N_B = \tilde{N}_C Z_B$ . Proceeding with the minimization, the only part of  $\mathcal{F}_{\mathcal{T}}$  that depends on  $\eta(\mathbf{r})$  is  $G$ . Minimizing with respect to  $\eta(\mathbf{r})$  is thus equivalent to

$$\frac{\delta}{\delta \eta(\mathbf{r})} G = 0 \quad , \quad (2.29)$$

which requires immediately

$$\sum_{\kappa=A,B,S} \frac{\rho_{\kappa}^0(\mathbf{r})}{\rho_{0\kappa}} = 1 \quad , \quad (2.30)$$

and hence

$$G = 0 \quad , \quad (2.31)$$

so that

$$\mathcal{F}_T^0 = F^0 \quad . \quad (2.32)$$

The only part of  $\mathcal{F}_T$  that depends on  $w_{\kappa}(\mathbf{r})$  is the corresponding  $\mathcal{Q}_{\kappa}$  and the integral involving the  $w_{\kappa}(\mathbf{r})$ . Minimizing  $\mathcal{F}_T$  with respect to  $w_{\kappa}(\mathbf{r})$  yields

$$\rho_{\kappa}^0(\mathbf{r}) + \frac{\tilde{N}_{\kappa}}{\mathcal{Q}_{\kappa}} \frac{\delta \mathcal{Q}_{\kappa}}{\delta w_{\kappa}(\mathbf{r})} = 0 \quad . \quad (2.33)$$

Comparison of Eq. (2.33) with Eqs. (2.26) and Eq. (2.27) gives the very important result that the saddle point values of  $\rho_{\kappa}^0(\mathbf{r})$ , which are what can be evaluated, are equal to the equilibrium density distributions  $\langle \hat{\rho}_{\kappa}(\mathbf{r}) \rangle$  in this approximation. The constraint of Eq. (2.28) becomes

$$\int d\mathbf{r} \rho_{\kappa}^0(\mathbf{r}) = N_{\kappa} \quad \kappa = S, A, B \quad . \quad (2.34)$$

## 2.4 Self-consistent Mean Field Theory of Tethered Polymer

The general assumptions discussed in section 2.3 result in equations for the density profiles of every component in the system and a free energy expression written in terms of the densities and interaction parameters. To obtain the density distributions for copolymer, one needs to solve the modified diffusion equation (2.17) for the propagators  $Q_{\kappa}(\mathbf{r}, \tau | \mathbf{r}', 0)$  subject to geometry-dependent initial and boundary conditions.

The problem has to be solved self-consistently. The potentials are needed to solve the diffusion equation and calculate the densities, but the potentials are functions of the densities.

Following the previous procedure, we are going to investigate the system studied by Kent *et al.* [7, 8, 12, 102], PDMS-PS spread as a monolayer at the free surface of EB. In this system EB is a good solvent for the PS block, and the air surface is repulsive for the PS. The PDMS (*A*-block) lies flat on the top of EB, and the PS (*B*-block) dangles into the solvent. All the *A* – *B* joints lie in a very narrow interphase region of width  $a$ , estimated by Kent [8] to be on the order of 1 nm for all samples. We have assumed that all the joints are randomly distributed throughout this interface.

By assuming that the system is translationally invariant parallel to the surface, the problem becomes one-dimensional. In order to specify the physical properties of the system, three density profiles should be determined: for the solvent, and for the *A* and the *B* blocks. The surface,  $x = 0$ , is defined as the plane at which the solvent and *B*-block densities reach zero.

If one is interested only in the properties of the dangling *B* block, one can simplify the problem by assuming a simple model for  $\phi_A(x)$ , such as [43]

$$\phi_A(x) = 1 - \tanh^2\left(\frac{x}{l}\right), \quad x \geq 0 \quad , \quad (2.35)$$

with the parameter  $l$  chosen to make the density profile for the anchored *A* block decrease to zero over the interface width of 1 nm.

One can then determine the density of the dangling *B*-block by using integral representations of the propagators given by the Eq. (2.16), where the integrations are performed over all starting positions [31]. Two propagators are needed. The first one is defined as

$$q_0(\mathbf{r}, \tau) = q_0(x, \tau) = \int d\mathbf{r}' Q_B(\mathbf{r}, \tau | \mathbf{r}', 0) \quad , \quad (2.36)$$

and the second one is

$$q_1(\mathbf{r}, \tau) = q_1(x, \tau) = \int d\mathbf{r}' d\mathbf{r}'' Q_A(\mathbf{r}'', Z_A|\mathbf{r}', 0) \mathcal{G}(\mathbf{r}') Q_B(\mathbf{r}, \tau|\mathbf{r}'', 0) \quad . \quad (2.37)$$

The propagators  $q_i$  also satisfy the diffusion equation

$$\left[ -\frac{b^2}{6} \frac{\partial^2}{\partial x^2} + w_B(x) \right] q_i(x, \tau) = -\frac{1}{Z_B} \frac{\partial}{\partial \tau} q_i(x, \tau) \quad , \quad (2.38)$$

with the variable  $\tau$  having been mapped onto the interval  $[0,1]$ . These propagators reflect the probability distribution of  $B$ -block of the chain. The first,  $q_0(x, \tau)$ , is proportional to the probability that a  $B$  chain of length  $\tau$  ends at  $x$  given that it starts somewhere in the system, while  $q_1(x, \tau)$  is proportional to the probability that a  $B$  chain of length  $\tau$  ends at  $x$  given that it starts in the interface.

In addition to satisfying the diffusion equation, the propagators satisfy certain boundary and initial conditions. If the surface is repulsive,  $\phi_B = 0$  at the upper edge of the interface region. One boundary condition, in this case, is then

$$q_i(0, \tau) = 0 \quad . \quad (2.39)$$

Also, since the chains can extend only a finite distance into the solvent, this implies that

$$q_i(\infty, \tau) = 0 \quad , \quad (2.40)$$

for the other boundary condition. In practice, this condition is applied at a finite distance, far enough to have no effect on the physical properties of the brush.

Since we assumed that the  $A - B$  joints are restricted within the interface of width of  $a$ , and distributed throughout it in a random way, this implies that the initial condition for  $q_1$  is given by

$$q_1(x, 0) = \begin{cases} 1, & 0 < x \leq a \\ 0, & x > a \end{cases} \quad . \quad (2.41)$$

Moreover, there are no restrictions on the position of the free end of  $B$  block, which leads to the initial condition for  $q_0$  given by

$$q_0(x, 0) = 1, \quad x > 0 \quad . \quad (2.42)$$

With these initial conditions, the integral of the distribution function, Eq. (2.19), becomes

$$\mathcal{Q} = \int_0^\infty dx q_1(x, 1) \quad . \quad (2.43)$$

According to this, the density of the dangling block can be expressed as

$$\phi_B(x) = \frac{Z_B}{\Sigma \rho_{\circ B} \mathcal{Q}} \int_0^1 d\tau q_1(x, \tau) q_0(x, Z - \tau) \quad . \quad (2.44)$$

In general, the monomers and solvent molecules interact with each other through some intermolecular potential, such as a Lennard-Jones or Morse type potential. However, in mean-field theories they are generally modelled as simple contact interactions, sometimes with a finite range correction. The result is that each pair interaction can be modelled by a single parameter, the Flory parameter,  $\chi_{\kappa\kappa'}$ , sometimes plus a gradient correction.

The self-consistent potential  $w_B(x)$ , which modifies the diffusion equation can be expressed using

$$\begin{aligned} w_B(x) = & \frac{\rho_{\circ S}}{\rho_{\circ B}} \left\{ \chi_{BS} \left[ \phi_S(x) - 1 - \phi_B(x) + \frac{\sigma^2}{6} \nabla^2 (\phi_S(x) - \phi_B(x)) \right] + \right. \\ & \left. (\chi_{AB} - \chi_{AS}) \left[ \phi_A(x) + \frac{\sigma^2}{6} \nabla^2 \phi_A(x) \right] \right\} + \\ & \frac{\rho_{\circ S}}{\rho_{\circ B}} \ln \frac{\phi_S^b}{\phi_S(x)} + u_B(x) - \frac{\rho_{\circ S}}{\rho_{\circ B}} u_S(x) \quad . \quad (2.45) \end{aligned}$$

Here, an additive constant has been chosen so that  $w(x) \rightarrow 0$  in the bulk, where  $\phi_S(x) = 1$ . In Eq. (2.45),  $\chi_{\kappa\kappa'}$ , is the Flory-Huggins interaction parameter between components  $\kappa$  and  $\kappa'$ , defined with  $\rho_{\circ S}$  as the reference density, and  $\phi_\kappa(x)$  is the volume fraction of  $\kappa$  component.

Since the experiments [7, 8] suggested there was little evidence of any particular affinity of the  $B$ -block for the grafted surface, both  $\chi_{AB}$  and  $\chi_{SA}$  should be positive and of comparable magnitude. In cases where the interactions with the surface are negligible, we can choose  $\chi_{AB} = \chi_{SA}$ , and neglect  $u_B(x) - [\rho_{oS}/\rho_{oB}]u_S(x)$ . The potential can then be written

$$w_B(x) = \frac{\rho_{oS}}{\rho_{oB}} \left\{ \ln \frac{1}{\phi_S(x)} + \chi_{SB} \left[ \phi_S(x) - \phi_B(x) - 1 + \frac{\sigma^2}{6} (\phi_S''(x) - \phi_B''(x)) \right] \right\} , \quad (2.46)$$

where  $\chi_{SB}$  has been defined using the solvent for the reference density.

Note that, in a bulk phase, only solvent is present,  $\rho_S^b = \rho_{oS}$  and the self-consistent potential for solvent has to be constant, which can be set to zero. It is

$$w_S(x) = \ln \left( \frac{1}{\phi_S(x)} \right) . \quad (2.47)$$

The parameter  $\sigma^2$ , whose dimensions are (length)<sup>2</sup>, characterizes the effective range of the interactions and its effects are usually very small. It can be chosen to be on the order of  $b^2$ , where  $b$  is the statistical segment length of the  $B$ -block. However,  $\sigma$  in this thesis has been set to zero.

Finally, to determine the density profile of the solvent, we use the incompressibility condition

$$\phi_S(x) = 1 - \phi_A(x) - \phi_B(x) . \quad (2.48)$$

In this model, and for a given copolymer system, which is characterized by  $\Sigma$ , which is the average area per polymer,  $Z_B$ ,  $\chi_{SB}$ ,  $\rho_{oS}$ , and  $\rho_{oB}$ , a self-consistent solution has to be obtained for the problem by the modified diffusion equation, and Eqs. (2.36) to (2.48).

In addition to the density profiles for each component of the system, the free energy of the brush is also of great interest. It is calculated using the terms in the free energy attributable to the  $B$  block.

The final expression for the free energy per unit area is given by

$$\frac{E_o}{\rho_{oS}K_B T} = \int_0^\infty dx \left\{ \phi_S(x) \ln \phi_S(x) + \phi_B(x) - \chi_{SB} \phi_B^2(x) - \frac{\rho_{oB}}{\rho_{oS}} w_B(x) \phi_B(x) \right\} - \frac{1}{\Sigma \rho_{oS}} \ln Q \quad . \quad (2.49)$$

In summary, we have a set of self-consistent equations describing the copolymer system through the use of the following assumptions:

1. Each bond in the chain of the copolymer has a Gaussian distribution, with an effective bond length referred to as statistical segment length.
2. The degrees of polymerization for the  $B$  block are assumed to be large so that the chain can be represented by a continuous space-curve.
3. No local volume change on mixing is allowed, which means that the system is incompressible.
4. The number of copolymer chains in the system is assumed to be large.
5. There are no fluctuations in the thermally averaged density distributions.
6. Only two-body interactions are taken into the account, and these interactions are assumed to act over a zero range,  $\sigma = 0$ .

# Chapter 3

## Lateral Compression - Excess Surface Pressure

### 3.1 Introduction

In this chapter the lateral compression of homopolymers and copolymers at the air-liquid interface is examined. Our investigation mimics the systems and methodology used by Kent *et al.* very closely. The difference is we use nSCF theory to generate the pressures, whereas they used experiments. We first describe in more detail the experiments of Kent *et al.* Next, we present the nSCF formalism, specific to the system being studied. Turning to the results, we first model adsorbed homopolymer, and calculate its contribution to the surface pressure. We then model the copolymer system, calculate  $\pi$ , and then the excess surface pressure,  $\Delta\pi$ . Our results are discussed in terms of power laws and compared with the experiments, other published calculations, and the previous results of Baranowski [72]. The chapter includes an analysis of different physical contributions to  $\Delta\pi$ .

### 3.1.1 Experimental Studies on the Lateral Compression of Copolymers at the Air-Liquid Interface

To examine the physical and the structural properties of copolymer systems at the air-liquid interface, Kent *et al.* [8, 12] conducted several experiments in which simultaneous measurements of concentration profiles and the surface pressure were carefully made. The diblock system PDMS-PS was found to spread and to form monolayers on the surface of ethyl-benzoate(EB), which is a good solvent for PS but nonsolvent for PDMS. This results in a system of tethered PS chains, with the PDMS at the surface. Moreover, the surface tension of EB lies between that of the PS and PDMS and this explains the selectivity of the solvent. Since  $\gamma_{PDMS} < \gamma_{EB}$ , there is a strong driving force for the PDMS-block to remain at the surface. By contrast,  $\gamma_{EB} < \gamma_{PS}$ , so PS dissolves into the bulk and does not adsorb at the surface.

Two methods of spreading the copolymer monolayers were used in the experiments. In most cases, the copolymers spread from a dry grain deposited onto the surface of the sub-phase. In the other cases, the spreading was accomplished using dilute solutions of the copolymers in chloroform, a good solvent for both blocks. This latter case provides better control over the surface coverage. The surface density was typically increased by adding further grains of copolymer to the surface, and decreased by aspirating the surface, rather than by compression and expansion of the surface area with a movable barrier. Virtually all the chains were adsorbed to the surface; the total volume fraction of copolymer in the bulk(sub-phase) was always estimated to be less than  $\sim 10^{-6}$ .

The spreading behavior of homopolymer (PS and PDMS) was also examined. When a dry grain of PS homopolymer was deposited onto the surface of EB, the PS did not spread to form a monolayer, but dissolved into the solvent after a short period

of time. As well, no change in the surface tension was noted throughout this process. This indicated that the PS was not active at the surface, and no adsorption occurred.

On the contrary, when a drop of PDMS homopolymer was deposited onto the surface of EB, the surface tension immediately dropped. This is due to the fact that the PDMS established a stable Langmuir monolayer on the surface of this solvent, and this indicated that the surface was attractive to the PDMS, which was active at the surface.

The surface pressure-area isotherms of PDMS on EB were obtained for two different samples of molecular weights, i.e.,  $M_w = 25,000$  and  $100,000$  (g/mol), and six different copolymers, which are 4-30 PDMS-PS, 10-40 PDMS-PS, 4.5-60 PDMS-PS, 21-169 PDMS-PS, 28-330 PDMS-PS, and 25-35 PDMS-PS, where the polymers are labeled by the block molecular weights, in kg/mol, of PDMS and PS blocks respectively. If the PS blocks' contribution to the surface pressure was small, then the isotherms for the copolymers would coincide with these of the PDMS homopolymer, the case which did not happen. It was found that, for most of the samples, there was a large deviation from the homopolymer isotherm; this indicated the effect of the PS block in raising the surface pressure.

As summarized earlier, Kent *et al.* measured both the homopolymer and copolymer surface pressure isotherms, and then calculated the excess surface pressure as the difference. They found that  $\Delta\pi$  increases relatively weakly with polymer coverage up to a certain threshold but, beyond that, it increases much more rapidly, still as a power law corresponding to powers that depend slightly on  $Z$ , but range from approximately 4.2 to 6.6 [8, 12].

In their study, Bijsterbosch *et al.* [11], used a series of PS-PEO diblock copolymers with different lengths of PEO block spread as a monolayers at the air-water interface. In order to get a full picture, both structural (neutron reflectivity) studies

and surface pressure measurements as a function of surface concentration of grafted chains,  $1/\Sigma$ , and chain lengths,  $Z$ , were done. The PEO-lengths which were used in the experiments were 90, 148, 250, 445, 700, 523.

The experimental results for the surface pressure versus surface area per monomer showed several distinguishable regions. At low concentrations, the system showed a low pressure analogue to the pressure for an ideal two-dimensional gas of polymers. At intermediate coverages, where the PEO block gradually forms a brush, the pressure is gently increasing. In the third region, where the surface coverages are high, and the brush is laterally compressed, the surface pressure begins to increase. Comparing the experimental results obtained by Bijsterbosch *et al.* [11], and the numerical calculations, using a double-logarithmical plot, Currie *et al.* [60] studied the surface pressure of the brush (excess pressure) against the area per chain for  $Z = 700$ . To determine the excess pressure for this system, they examined the surface pressure for the saturated adsorbed homopolymer of PEO-chains, which was reported in experiments to be equal to 9.8 mN/m, while it was estimated by the nSCF model to be 8.2 mN/m. The power law exponent for the excess pressure as a function of grafting density is found to be  $5/3 \approx 1.67$ , if the surface pressure for the PEO homopolymer solution was taken to be 9.8 mN/m. This result is exactly the same as predicted by aSCF model, and close to the scaling theory prediction of  $\approx 1.83$ . The procedure used by Currie *et al.* to find the excess surface pressure for this system is to take the saturated surface pressure of a solution of long PEO chains, which is reported experimentally to be equal to 9.8 mN/m, and then subtract this value from the surface pressure of the PS-PEO copolymer measured in Bijsterbosch's experiments. They used this method since the PS block is known not to spread on water, which means its contribution to the surface pressure is very little, while PEO blocks, which spread on the water surface, contribute more to the surface pressure. So in these

experiments, as the density of PS-PEO copolymer increases, the PEO blocks start to aggregate near the surface, and contribute to the surface pressure similar to the PEO homopolymer solution. When the pressure reaches a value of approximately 10 mN/m, at which the surface density of PEO has reached its plateau, and upon further compression, the free ends of the PEO blocks start to extend into the solution and form a brush. So by using the previous procedure, we get only the excess surface pressure due to the dangling blocks of PEO. The experiments showed no evidence of a rapid raise in the surface pressure excess as reported by Kent *et al.* [12]. Instead, results are consistent with values predicted by aSCF theory [41, 87].

### 3.2 Numerical Self-Consistent-Field Approach

The general formalism for the nSCF theory was presented in chapter 2, in which we considered only the dangling block to be of interest. This assumption is responsible for the simple model of the adsorbed *A*-block(PDMS). However, in this chapter, we study the surface pressure of copolymers and homopolymers at the air-liquid surface, and the behavior of both blocks must be taken into account. Two cases have to be examined. The first is the pure homopolymer at the interface. The second is the diblock copolymer, in which the *A*-block is similar to the homopolymer, and the *B*-block is dangling into the solution. In order to probe the thermodynamic and structural properties of both cases, the density distributions and the free energy of the system have to be calculated. For the copolymers, the density distributions of both blocks are to be determined self-consistently.

### 3.2.1 The Homopolymer Spread as a Monolayer

We consider a system comprised of  $\tilde{N}_{HA}$  identical homopolymer chains (PDMS) described by the density of the pure material,  $\rho_{oA}$ , statistical segment length,  $b_A$ , and degree of polymerization,  $Z_A$ , and  $\tilde{N}_S$  solvent molecules (EB) characterized by  $\rho_{oS}$ . The partition function, Eq. (2.6), has the same form, with a few changes:  $\tilde{N}_C$  has to be replaced by  $\tilde{N}_{HA}$ , and the summation is restricted to one type of molecules: A type. Similarly, since the polymer consists of one type of monomer, then the condition of connectivity should be dropped, and the  $\delta(\dots)$  function has to be eliminated. Following the formalism of Eqs. (2.8)-(2.17), the integral of the distribution function, Eq. (2.19), can be written as

$$\mathcal{Q}_H = \int d\mathbf{r} d\mathbf{r}' \mathbf{Q}_A(\mathbf{r}, Z_A | \mathbf{r}', 0) \mathcal{G}(\mathbf{r}'(0)) \quad . \quad (3.1)$$

The density distribution of the homopolymer is given by

$$\rho_A(\mathbf{r}) = \frac{\tilde{N}_{HA}}{\mathcal{Q}_H} \int_0^{Z_A} d\tau \left\{ \int d\mathbf{r}' d\mathbf{r}'' \mathbf{Q}_A(\mathbf{r}, \tau | \mathbf{r}'', 0) \mathcal{G}(\mathbf{r}''(0)) \mathbf{Q}_A(\mathbf{r}', (Z_A - \tau) | \mathbf{r}, \tau) \right\} \quad . \quad (3.2)$$

The problem is considered as one dimensional, as before, which means the system is assumed to be translationally invariant parallel to the interface. Using the integral representation of the propagators, we can write the second propagator  $q_{1A}$  as

$$q_{1A}(\mathbf{r}, \tau) = q_1(x, \tau) = \int d\mathbf{r}' \mathbf{Q}_A(\mathbf{r}, \tau | \mathbf{r}', 0) \mathcal{G}(\mathbf{r}') \quad , \quad (3.3)$$

and the initial condition for this propagator is

$$q_{1A}(x, 0) = \int d\mathbf{r}' \delta(\mathbf{r} - \mathbf{r}') \mathcal{G}(\mathbf{r}') = \mathcal{G}(x) \quad . \quad (3.4)$$

It should be noted that both propagators satisfy the diffusion equation, Eq. (2.38).

Since in the experiments of Kent [12] the homopolymer forms a monolayer, it is

possible to assume that one end of every chain starts in the vicinity of the surface, so taking this into account, the propagator  $q_{1A}(x, 0)$  is assumed to satisfy

$$q_{1A}(x, 0) = \exp(-a_1 x^2) \quad , \quad (3.5)$$

where Baranowski [72] chose  $a_1$  so that  $q_{1A}(1, 0) = 0.01$  at a distance of 1 nm from the surface. This choice is compatible with the estimated thickness of the interface which was on the order of 1 nm [72]. Some of the calculations in this thesis were done to test the effects of this choice. It was concluded that the results were not sensitive to it.

In terms of  $q_{0A}(x, \tau)$  and  $q_{1A}(x, 0)$  the quantity  $\mathcal{Q}_H$  can be expressed as

$$\begin{aligned} \mathcal{Q}_H &= \int d\mathbf{r} d\mathbf{r}' \mathbf{Q}_H(\mathbf{r}, Z|\mathbf{r}') \mathcal{G}(\mathbf{r}') \\ &= \int dx dy dz q_1(x, Z) = \mathcal{A} \int_0^\infty dx q_1(x, Z_A) \\ &= \mathcal{A} \mathcal{Q}_H^x \quad , \end{aligned} \quad (3.6)$$

where  $\mathcal{A}$  is the total area of the adsorbing surface and the boundaries of the integral sweep out all possible locations of the mobile end of the homopolymer.

Another important quantity that is needed is the local volume fraction of homopolymer. It is given by

$$\phi_A(x) = \frac{Z_{HA}}{\rho_{oA} \Sigma \mathcal{Q}_H^x} \int_0^1 d\tau q_{0A}(x, \tau) q_{1A}(x, 1 - \tau) \quad , \quad (3.7)$$

where  $\tau$  has been mapped onto  $[0, 1]$ .

The concentration profile of the polymer in the vicinity of the surface depends on the nature of interaction between the chain and the interface. For a repulsive surface, a polymer depletion layer is found near the surface. On the other hand, there will be adsorption for the polymer if the surface prefers the polymer molecules to the solvent, in which attractive interaction is dominant. According to the results of many

experiments conducted to study polymer systems, it can be assumed that, at  $x = 0$ , the density profile shows a local extremum (minimum or maximum) which implies

$$\left. \frac{\partial}{\partial x} q_{iA}(x, \tau) \right|_{x=0} = 0 \quad , \quad (3.8)$$

for  $i = 0, 1$ . This boundary condition eliminates all configurations which cross the surface. Similarly, for the other boundary in the pure bulk it is set

$$\left. \frac{\partial}{\partial x} q_{iA}(x, \tau) \right|_{x=\infty} = 0 \quad . \quad (3.9)$$

In practice, this boundary condition is applied at some finite distance,  $L$ . This distance must be chosen to be large enough so that the calculated polymer density is zero at  $x = L$ .

The potential which modifies the diffusion equation Eq. (2.38) for the homopolymer calculations is given by

$$\begin{aligned} w_A(x) &= \frac{\rho_{oS}}{\rho_{oA}} \chi_{AS} \left[ \phi_S(x) - 1 - \phi_A(x) \right] + \frac{\rho_{oS}}{\rho_{oA}} \ln \frac{1}{\phi_S(x)} + u_A(x) - \frac{\rho_{oS}}{\rho_{oA}} u_S(x) \\ &= w_A^{int}(x) + \frac{\rho_{oS}}{\rho_{oA}} \ln \frac{1}{\phi_S(x)} + u_A(x) - \frac{\rho_{oS}}{\rho_{oA}} u_S(x) \quad , \end{aligned} \quad (3.10)$$

which was obtained in the same manner as Eq. (2.45). The parameter  $\sigma^2$ , which characterizes the effective range of the interactions was, for simplicity, set to zero.

### 3.2.2 Diblock Copolymer at the Air-Liquid Interface

In this section the formalism for the diblock copolymer (PDMS-PS) at the air-liquid interface of solvent (EB) is introduced. The diblock consists of a block  $A$  characterized by degree of polymerization,  $Z_A$ , statistical length,  $b_A$ , and the density of pure material,  $\rho_{oA}$ . Similarly, block  $B$  can be specified by  $Z_B$ ,  $b_B$ , and  $\rho_{oB}$ , and the solvent by its density,  $\rho_{oS}$ . Moreover, it is assumed that all the chains in the system are adsorbed at the interface. This situation is consistent with Kent *et al.* [8, 12] in

which the total concentration of the copolymer in the bulk was negligible. The total number of copolymer chains adsorbed at the interface is  $\tilde{N}_C$  and the total number of solvent molecules in the system is  $\tilde{N}_S$ . Both of the blocks are responsible for the total surface pressure,  $\pi$ .

The adsorbed *A*-block is the same as the homopolymer considered in the previous section. The density distribution for the *A*-block of the copolymer is given by

$$\rho_A(\mathbf{r}) = \frac{\tilde{N}_C}{\mathcal{Q}_C} \int_0^{Z_A} d\tau \left\{ \int d\mathbf{r}' d\mathbf{r}'' d\mathbf{r}''' \mathbf{Q}_A(\mathbf{r}, \tau | \mathbf{r}', 0) \mathcal{G}(\mathbf{r}') \right. \\ \left. \mathbf{Q}_A(\mathbf{r}'', (Z_A - \tau) | \mathbf{r}, \tau) \mathbf{Q}_B(\mathbf{r}'', Z_B | \mathbf{r}''', 0) \right\} . \quad (3.11)$$

Similarly, the *B*-block density distribution is given by

$$\rho_B(\mathbf{r}) = \frac{\tilde{N}_C}{\mathcal{Q}_C} \int_0^{Z_B} d\tau \left\{ \int d\mathbf{r}' d\mathbf{r}'' d\mathbf{r}''' \mathbf{Q}_A(\mathbf{r}'', Z_A | \mathbf{r}', 0) \mathcal{G}(\mathbf{r}') \right. \\ \left. \mathbf{Q}_B(\mathbf{r}, \tau | \mathbf{r}'', 0) \mathbf{Q}_B(\mathbf{r}''', (Z_B - \tau) | \mathbf{r}, \tau) \right\} . \quad (3.12)$$

It should be noted that these density distribution functions are calculated at the saddle point. It is useful to use the integral representation of the propagators in which one integrates over all possible starting positions. In the copolymer/solvent system, four propagators are needed. The first one, denoted  $q_A(x, \tau)$ , is defined as

$$q_A(\mathbf{r}, \tau) = q_A(x, \tau) = \int d\mathbf{r}' \mathbf{Q}_A(\mathbf{r}, \tau | \mathbf{r}', 0) \mathcal{G}(\mathbf{r}'(0)) . \quad (3.13)$$

Since it is assumed that the free end of the *A*-block is located near the surface, this means that Eq. (3.13) is identical to Eq. (3.3) and satisfies the same initial conditions, Eq. (3.4) or Eq. (3.5). The second propagator,  $q_B(x, \tau)$  is defined as

$$q_B(\mathbf{r}, \tau) = q_B(x, \tau) = \int d\mathbf{r}' \mathbf{Q}_B(\mathbf{r}, \tau | \mathbf{r}', 0) . \quad (3.14)$$

This propagator  $q_B(\mathbf{r}, \tau)$  express the fact that the free end of the dangling *B*-block is not localized, and can be found anywhere in solution. Another two propagators are

needed, and are defined as follows:

$$\tilde{q}_A(\mathbf{r}, \tau) = \tilde{q}_A(x, \tau) = \int d\mathbf{r}' \mathbf{Q}_A(\mathbf{r}, \tau | \mathbf{r}') q_B(\mathbf{r}', Z_B) \quad , \quad (3.15)$$

and

$$\tilde{q}_B(\mathbf{r}, \tau) = \tilde{q}_B(x, \tau) = \int d\mathbf{r}' \mathbf{Q}_B(\mathbf{r}, \tau | \mathbf{r}', 0) q_A(\mathbf{r}', Z_A) \quad . \quad (3.16)$$

The initial conditions for any point within the semi-infinite region,  $x > 0$ , are

$$\tilde{q}_A(x, 0) = q_B(x, Z_B) \quad , \quad (3.17)$$

for  $\tilde{q}_A$  and

$$\tilde{q}_B(x, 0) = q_A(x, Z_A) \quad , \quad (3.18)$$

for the propagator  $\tilde{q}_B$ . As we assumed for the homopolymer, these propagators also satisfy the same boundary conditions as previously, Eqs. (3.8) and (3.9). The densities can be re-written in terms of the propagators  $q$  and  $\tilde{q}$  as

$$\phi_A(x) = \frac{Z_A}{\Sigma \mathcal{Q}_C^x \rho_{\circ A}} \int_0^1 d\tau q_A(x, \tau) \tilde{q}_A(x, 1 - \tau) \quad (3.19)$$

$$\phi_B(x) = \frac{Z_B}{\Sigma \mathcal{Q}_C^x \rho_{\circ B}} \int_0^1 d\tau q_B(x, \tau) \tilde{q}_B(x, 1 - \tau) \quad . \quad (3.20)$$

The integral of the distribution functions,  $\mathcal{Q}_C$ , Eq. (2.19), becomes

$$\mathcal{Q}_C = \mathcal{A} \int_0^\infty dx q_A(x, Z_A) q_B(x, Z_B) = \mathcal{A} \mathcal{Q}_C^x \quad . \quad (3.21)$$

The self-consistent potential, which modifies the diffusion equation for the propagators for the  $A$  block is given by

$$\begin{aligned} w_A(x) &= \frac{\rho_{\circ S}}{\rho_{\circ A}} \left\{ \chi_{AS} \left[ \phi_S(x) - 1 - \phi_A(x) \right] + \phi_B(x) \left[ \chi_{AB} - \chi_{BS} \right] + \ln \frac{1}{\phi_S(x)} \right\} \\ &\quad + u_A(x) - \frac{\rho_{\circ S}}{\rho_{\circ A}} u_S(x) \\ &\equiv w_A^{int}(x) + \frac{\rho_{\circ S}}{\rho_{\circ A}} \ln \frac{1}{\phi_S(x)} + u_A(x) - \frac{\rho_{\circ S}}{\rho_{\circ A}} u_S(x) \quad , \end{aligned} \quad (3.22)$$

where  $w_A^{int}(x)$  represents the interaction with solvent and the  $B$  block,  $u_A(x)$  is the surface- $A$ -block interaction potential, and  $u_S(x)$  is the surface-solvent interaction potential. The potential for the  $B$  block propagators is obtained from this expression by interchanging  $A$  and  $B$ .

### 3.2.3 The Model of the Interaction with the Surface

In the models used in this thesis, the planar surface is smooth, lacking the molecular roughness of a real surface. As a result, the problem is translationally invariant parallel to the surface, and the problem is one dimensional. Hence, the surface potential due to the presence of the surface depends on the linear distance  $x$  from the surface, and can be described in the mean-field model through energy and length parameters.

Eq. (3.22) includes the interactions of the homopolymer or one block of the copolymer with the surface, and the interactions of the solvent with the surface. It follows from this equation that the effective surface-polymer potential i.e., external potential acting on the block  $\kappa$ , can be introduced as

$$\begin{aligned} u_\kappa^{eff}(x) &= w_\kappa(x) - w_\kappa^{int}(x) - \frac{\rho_{oS}}{\rho_{o\kappa}} \ln \frac{1}{\phi_S(x)} \\ &= u_\kappa(x) - \frac{\rho_{oS}}{\rho_{o\kappa}} u_S(x) \end{aligned} \quad (3.23)$$

According to the behavior of homopolymer or one block of copolymer in a vicinity of the surface, we can distinguish between three types of surfaces: attractive, repulsive, and neutral.

If  $u_\kappa^{eff}(x)$  is attractive and arises from Lennard-Jones interactions between the surface and the molecules in the solution, then the long-range part of potential is of the form [109]

$$u_\kappa^{eff}(x) \propto -\frac{1}{x^3} \quad (3.24)$$

For an attractive surface it can be modeled as

$$u_{\kappa}^{eff}(x) = \begin{cases} -\chi_S & \text{for } x \leq l \\ -\chi_S \left(\frac{x}{l}\right)^{-3} & \text{for } x > l \end{cases} \quad (3.25)$$

where  $\chi_S$  is the energy (in units of  $k_B T$ ) and  $l$  is the length parameter. For the dangling block of a copolymer, we chose  $u_B^{eff}(x) = 0$ , because the density of the dangling block very close to the surface is nearly zero.

### 3.2.4 Free Energy of the System, Interfacial Tension and Surface Pressure

The general expression for the free energy of the copolymer/solvent system at the air-liquid interface was derived in Chapter 2, and is given by Eq. (2.22). The potential energy of the system,  $W[\{\rho_{\kappa}(\cdot)\}]$ , is given by

$$W = \frac{1}{2} \sum_{\kappa=A,B,S} W_{\kappa\kappa} \rho_{\kappa} N_{\kappa} + \frac{1}{2} \rho_{oS} \sum_{\kappa,\kappa'} \chi_{\kappa\kappa'} \int d\mathbf{r} \phi_{\kappa}(\mathbf{r}) \phi_{\kappa'}(\mathbf{r}) + \sum_{\kappa=A,B,S} \int d\mathbf{r} \rho_{\kappa} \phi_{\kappa}(\mathbf{r}) u_{\kappa}(\mathbf{r}) \quad , \quad (3.26)$$

where

$$W_{\kappa\kappa} = \int d\mathbf{r} W_{\kappa\kappa}(\mathbf{r}) \quad , \quad (3.27)$$

which is a measure of the overall strength of the interaction.

In order to find the free energy, we substitute this equation in addition to Eq. (3.22) for the self-consistent potentials,  $w_{\kappa}(x)$ , into Eq. (2.22). This yields

$$F = \frac{1}{2} \sum_{\kappa=A,B,S} W_{\kappa\kappa} \rho_{\kappa} N_{\kappa} + \tilde{N}_S \left( \ln \frac{\rho_{oS}}{\mathcal{Z}_S} - 1 \right) + \tilde{N}_C \left( \ln \frac{\tilde{N}_C}{Q_C \mathcal{Z}_C} - 1 \right) + \mathcal{A} \rho_{oS} \int_0^{\infty} dx \left\{ \frac{1}{2} \sum_{\kappa,\kappa'} \chi_{\kappa\kappa'} \phi_{\kappa}(x) \phi_{\kappa'}(x) + \phi_S(x) \ln \phi_S(x) - \sum_{\kappa=A,B} \frac{\rho_{\kappa}}{\rho_{oS}} w_{\kappa}^{int}(x) \phi_{\kappa}(x) + u_S(x) \right\} \quad , \quad (3.28)$$

where  $\tilde{N}_S/Q_S = \rho_{oS}$ .

For a pure system of  $\tilde{N}_S$  molecules and the surface, this free energy expression has the simple form

$$F_S = \frac{1}{2}W_{SS}\rho_{oS}N_S + N_S \left( \ln \frac{\rho_{oS}}{Z_S} - 1 \right) + A\rho_{oS} \int_0^\infty dx u_S(x) \quad (3.29)$$

Using this simple form, the free energy Eq. (3.28) can be written as

$$\begin{aligned} F = & F_S + \frac{1}{2} \sum_{\kappa=A,B} W_{\kappa\kappa}\rho_{o\kappa}N_\kappa + \tilde{N}_C \left( \ln \frac{\tilde{N}_C}{Q_C Z_C} - 1 \right) \\ & + A\rho_{oS} \int_0^\infty dx \left\{ \frac{1}{2} \sum_{\kappa,\kappa'} \chi_{\kappa\kappa'} \phi_\kappa(x) \phi_{\kappa'}(x) + \phi_S(x) \ln \phi_S(x) \right. \\ & \left. - \sum_{\kappa=A,B} \frac{\rho_{o\kappa}}{\rho_{oS}} w_\kappa^{int}(x) \phi_\kappa(x) \right\} \quad (3.30) \end{aligned}$$

Since the densities and the potentials depend on the linear distance from the surface,  $x$ , one can divide Eq. (3.30) by the total area of the interface to get the free energy per unit area,  $f = F/A$ . In units of  $k_B T$ ,  $f$  can be written as

$$\begin{aligned} f = & f_S + \frac{1}{2} \frac{1}{\Sigma} \sum_{\kappa=A,B} W_{\kappa\kappa}\rho_{o\kappa}Z_\kappa + \frac{1}{\Sigma} \left( \ln \frac{1}{\Sigma Q_C^x Z_C} - 1 \right) \\ & + \rho_{oS} \int_0^\infty dx \left\{ \frac{1}{2} \sum_{\kappa,\kappa'} \chi_{\kappa\kappa'} \phi_\kappa(x) \phi_{\kappa'}(x) + \phi_S(x) \ln \phi_S(x) \right. \\ & \left. - \sum_{\kappa=A,B} \frac{\rho_{o\kappa}}{\rho_{oS}} w_\kappa^{int}(x) \phi_\kappa(x) \right\} \quad (3.31) \end{aligned}$$

where  $\Sigma = (\tilde{N}_C/A)^{-1}$ .

The free energy of the multicomponent system with a surface can be written as a Legendre transform of the internal energy with respect to entropy, which can be written as

$$F = \sum_{\kappa} \mu_\kappa N_\kappa - PV + \gamma A \quad (3.32)$$

and its total differential as

$$dF = -PdV - SdT + \sum_{\kappa} \mu_\kappa dN_\kappa + \gamma dA \quad (3.33)$$

where  $\mu_\kappa$  is the chemical potential of the  $\kappa$  component. In this representation, the interfacial tension,  $\gamma$ , is defined as the change in the total free energy when the interfacial area,  $\mathcal{A}$ , is increased at constant temperature  $T$ , total volume of the system,  $V$ , and constant numbers of particles in the system,  $N_i$ . Since the free energy per unit area, and the volume fractions of all components all depend explicitly on  $\Sigma$ , rather than the total area of the interface,  $\mathcal{A}$ , it is convenient to express the interfacial tension,  $\gamma$ , as

$$\begin{aligned}\gamma &= \left(\frac{\partial F}{\partial \mathcal{A}}\right)_{T,V,N_\kappa} \\ &= f + \mathcal{A} \left(\frac{\partial f}{\partial \mathcal{A}}\right)_{T,V,N_\kappa} \\ &= f + \tilde{N}_C \Sigma \left(\frac{\partial f}{\partial \Sigma}\right)_{T,V,\mathcal{A}} \left(\frac{\partial \Sigma}{\partial \mathcal{A}}\right)_{T,V,N_\kappa}\end{aligned}\quad (3.34)$$

Since  $\mathcal{A} = \tilde{N}_i \Sigma$  ( $i$  can be homopolymer,  $H$ , or diblock copolymer,  $C$ ), the result for constant  $T$  and  $V$  is

$$\gamma = f + \Sigma \left(\frac{\partial f}{\partial \Sigma}\right)_{T,V,\mathcal{A}} \quad (3.35)$$

It is apparent from Eq. (3.35), that all terms in  $f$  which are linear in  $1/\Sigma$  do not contribute to  $\gamma$ .

For a pure solvent

$$\gamma_S = \rho_{oS} \int_0^\infty dx u_S(x) \quad , \quad (3.36)$$

where  $u_S(x)$  is the external potential due the interactions between the solvent molecules and the interface. With this, the expression for the interfacial tension can be written as

$$\gamma = \gamma_S + \mathcal{L} + \Sigma \frac{\partial \mathcal{L}}{\partial \Sigma} \quad , \quad (3.37)$$

where  $\mathcal{L}$  is given by

$$\mathcal{L} = \frac{1}{\Sigma} \ln \left( \frac{1}{\Sigma Q_C^x} \right) + \rho_{oS} \int_0^\infty dx \left\{ \frac{1}{2} \sum_{\kappa, \kappa'} \chi_{\kappa\kappa'} \phi_\kappa(x) \phi_{\kappa'}(x) + \phi_S(x) \ln \phi_S(x) \right\}$$

$$- \sum_{\kappa=A,B} \frac{\rho_{\circ\kappa}}{\rho_{\circ S}} w_{\kappa}^{int}(x) \phi_{\kappa}(x) \} . \quad (3.38)$$

As was mentioned before, the change in the surface tension  $\gamma_S - \gamma$  can be interpreted as a two-dimensional pressure, referred to as the surface pressure

$$\pi = \gamma_S - \gamma , \quad (3.39)$$

which, according to the formalism presented above, has the form

$$\pi = -\mathcal{L} - \Sigma \frac{\partial \mathcal{L}}{\partial \Sigma} . \quad (3.40)$$

If a constant value is added to the self-consistent potentials, the results will be the same. Taking this into account, and choosing the potentials of the  $A$  and  $B$ -blocks so that

$$\int_0^{\infty} dx w_{\kappa}(x) \phi_{\kappa}(x) = 0, \quad \kappa = A, B , \quad (3.41)$$

then Eq. (3.38) can be written in detailed form as

$$\begin{aligned} \mathcal{L} = & \rho_{\circ S} \int_0^{\infty} dx \left\{ \frac{\rho_{\circ A}}{\rho_{\circ S}} \phi_A(x) u_A^{eff}(x) + \frac{\rho_{\circ B}}{\rho_{\circ S}} \phi_B(x) u_B^{eff}(x) \right\} + \\ & + \rho_{\circ S} \int_0^{\infty} dx \left\{ \chi_{AB} \phi_A(x) \phi_B(x) + \chi_{AS} \phi_A(x) \phi_S(x) + \chi_{BS} \phi_B(x) \phi_S(x) \right\} \\ & + \frac{1}{\Sigma} \ln \left( \frac{1}{\Sigma Q_C^x} \right) + \rho_{\circ S} \int_0^{\infty} dx \phi_S(x) \ln \phi_S(x) . \end{aligned} \quad (3.42)$$

This equation can be interpreted physically. The first line represents the contribution due to the external potential which arises from the interactions of all components of the system with the surface, the second line is the interaction energy within these components, and the third line expresses the entropic contribution to the free energy. This latter part includes effects due to chain conformations, chain localization and solvent distribution. With this physical interpretation, Eq. (3.42) can be written as

$$\mathcal{L} = \mathcal{L}_{ext}(\Sigma) + \mathcal{L}_{int}(\Sigma) + \mathcal{L}_{ent}(\Sigma) . \quad (3.43)$$

Using the condition of no local volume change upon mixing (incompressibility), and setting  $u_B^{eff}(x) = 0$ , the first contribution can be written as

$$\mathcal{L}_{ext}(\Sigma) = \int dx \rho_{oA} \phi_A(x) u_A^{eff}(x) \quad . \quad (3.44)$$

Equations (3.42) and (3.43) are applicable to the homopolymer/solvent system with appropriate modifications. Namely, for the homopolymer/solvent system,  $\mathcal{Q}_C^x$  in the entropic part has to be replaced by  $\mathcal{Q}_H^x$ , and in the  $\mathcal{L}_{int}$ , since there is one type of blocks, there are no terms for  $AB$  and  $BS$  interactions. In the  $\mathcal{L}_{ext}$ , for the homopolymer, there will appear only one type of block, and this part can be referred to as the anchoring energy.

### 3.2.5 Approximations in Earlier nSCF Calculations

As mentioned before, Baranowski used an approximation in his calculations in order to model Kent's experiments. First, he chose  $a_1$ , appearing in Eq. (3.5), which is the localization of the end of adsorbed block, so that  $q_{1A} = 0.01$  at a distance of 1 nm from the surface. Second, the calculations are, in principle, for a semi-infinite region  $[0, \infty]$ . In practice, we use a finite region  $[0, L]$ . The boundary conditions are then applied at  $x = L$  instead of  $x = \infty$ , and spatial integrations carried over this finite interval.  $L$  must be chosen large enough that its presence does not affect the tethered polymers. Otherwise, it is equivalent to a second surface located at  $x = L$ .

## 3.3 Results and Discussion

In this section, numerical results for PDMS homopolymer, and PDMS-PS at the EB/air interface are presented, discussed, and compared to the experimental data of Kent *et al.*[8,12]. Calculations were performed for two homopolymers, and six

copolymers. For each polymer, different surface densities were examined. The overall range in  $\Sigma$  was from on the order of 10 to 5000 nm<sup>2</sup> per chain. The densities were  $\rho_{oS} = 4.21$  molecules/nm<sup>3</sup> for EB,  $\rho_{oA} = 7.89$  monomers/nm<sup>3</sup> for the *A*-block (PDMS), and  $\rho_{oB} = 6.2$  monomers/nm<sup>3</sup> for the *B*-block (PS). Since the observed radius of gyration of PS in EB is very similar to that in toluene (TOL), the measured PS-TOL interaction parameter, i.e.,  $\chi_{BS} = 0.44$  was used. For the same reason,  $b_B = 0.71$  nm was chosen for the statistical segment length for the dangling block. For the anchored block,  $b_A = 0.57$  nm [72]. In the experiments, Kent *et al.* [8, 12] used

$$R_g = 0.0117M_w^{0.595} \quad , \quad (3.45)$$

for the radius of gyration  $R_g$  of an isolated PS, where  $M_w$  is the (weight averaged) molecular weight, and the same expression was used here to calculate the reduced surface coverage,  $\sigma^*$ , for each  $\Sigma$ . It should be noted that the use of this expression is not fundamental but it provides a way of analyzing the results and comparing them to the experiments. Furthermore, the interaction parameters of systems under investigation were either measured or chosen in a reasonable way. The PDMS-EB interaction parameter has not been measured [72]. Given that EB is a non-solvent for PDMS, then  $\chi_{AS} = 0.7$  was used. The PDMS and PS polymers are not compatible and again, a reasonable interaction parameter was chosen, and as such  $\chi_{AB} = 0.1$  was used, which is typical of diblock copolymer systems [72]. Since the *A*-block of copolymer is confined to the narrow interface, and there is a little overlap between *A* and *B* blocks, the results should not be sensitive to these choices of  $\chi_{AS}$  and  $\chi_{AB}$  parameters.

Furthermore, and due to the fact the *B*-block is extending into the solution and is not active at the surface, it was assumed that  $u_B^{eff}$  is negligible and was set to zero everywhere.

The surface is attractive for the PDMS, so  $u_A^{eff}$  was chosen to be of the same form as Eq. (3.25). The parameters,  $\chi_S$  and  $l$ , were based on many numerical calculations, to produce the best description of the surface pressure isotherm for the homopolymer presented in the next section [72]. The result was

$$u_{\kappa}^{eff}(x) = \begin{cases} -0.4505 & \text{for } x \leq 0.7 \text{ nm} \\ -0.4505 \left(\frac{x}{0.7}\right)^{-3} & \text{for } x > 0.7 \text{ nm} \end{cases} \quad (3.46)$$

For each system under investigation, which is characterized by the values of degree of polymerization of the homopolymer or the two blocks of the copolymer, the material characteristics presented above, and the average number of chains per unit area,  $1/\Sigma$ , the self-consistent solution is found. The free energy of the system, Eq. (3.42), is then calculated. The surface pressure isotherms as a function of the surface coverage are obtained by the numerical evaluation of Eq. (3.40).

### 3.3.1 Surface Pressure Isotherms - Homopolymer

To investigate the homopolymer at the interface, numerical calculations for two PDMS homopolymers specified by  $M_w = 25,000$  and  $M_w = 50,000$  g/mol ( $Z_A = 337$  and  $675$  respectively) at the surface of EB were performed. For each homopolymer, the adsorbed amount,  $\Gamma_A = Z_A/\Sigma$ , was varied from just above 0 to almost 19 monomers/nm<sup>2</sup>. This value is an input to the SCF calculation. The adsorbed amount can also be calculated from the final solution, through

$$\Gamma_A = \rho_{\circ A} \int_0^{\infty} dx [\phi_A(x) - \phi_A^b] \quad , \quad (3.47)$$

with  $\phi_A^b = 0$ . The difference between the results obtained by  $\Gamma_A = Z_A/\Sigma$  and that obtained by Eq. (3.47) is one measure of the accuracy of the numerical calculations. In all the calculations presented here this difference was less than  $1 \times 10^{-5}\%$ .

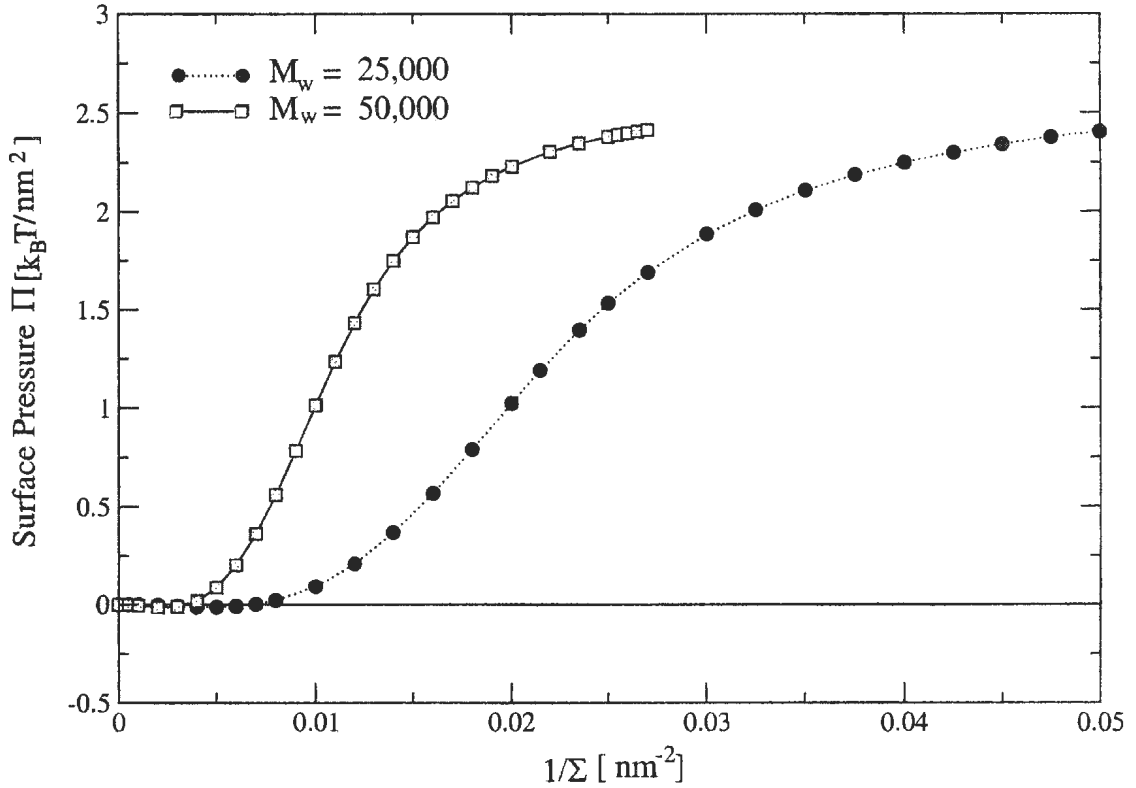


Figure 3.1: Surface pressure  $\pi$  as a function of the number of adsorbed chains per unit area for PDMS homopolymers,  $M_w = 25,000$  and  $M_w = 50,000$ . (The lines are guides to the eye).

Figure 3.1 shows the surface pressure isotherms for these two homopolymers, as a function of the number of adsorbed chains per unit area,  $1/\Sigma$ . As expected, as the area per adsorbed chain decreases, i.e., the chains start to accumulate close to each other, then the surface pressure rises, but at high surface coverages it begins to level off. This occurs at  $1/\Sigma \simeq 0.04 \text{ nm}^{-2}$  and  $1/\Sigma \simeq 0.02 \text{ nm}^{-2}$  for  $M_w = 25,000$  and  $M_w = 50,000$  homopolymer, respectively.

In Figure 3.2, comparison between numerical results of the surface pressure isotherms for the two PDMS homopolymers as a function of the adsorbed amount,  $\Gamma_A$  are presented. In this comparison, the isotherms are identical, indicating that they are

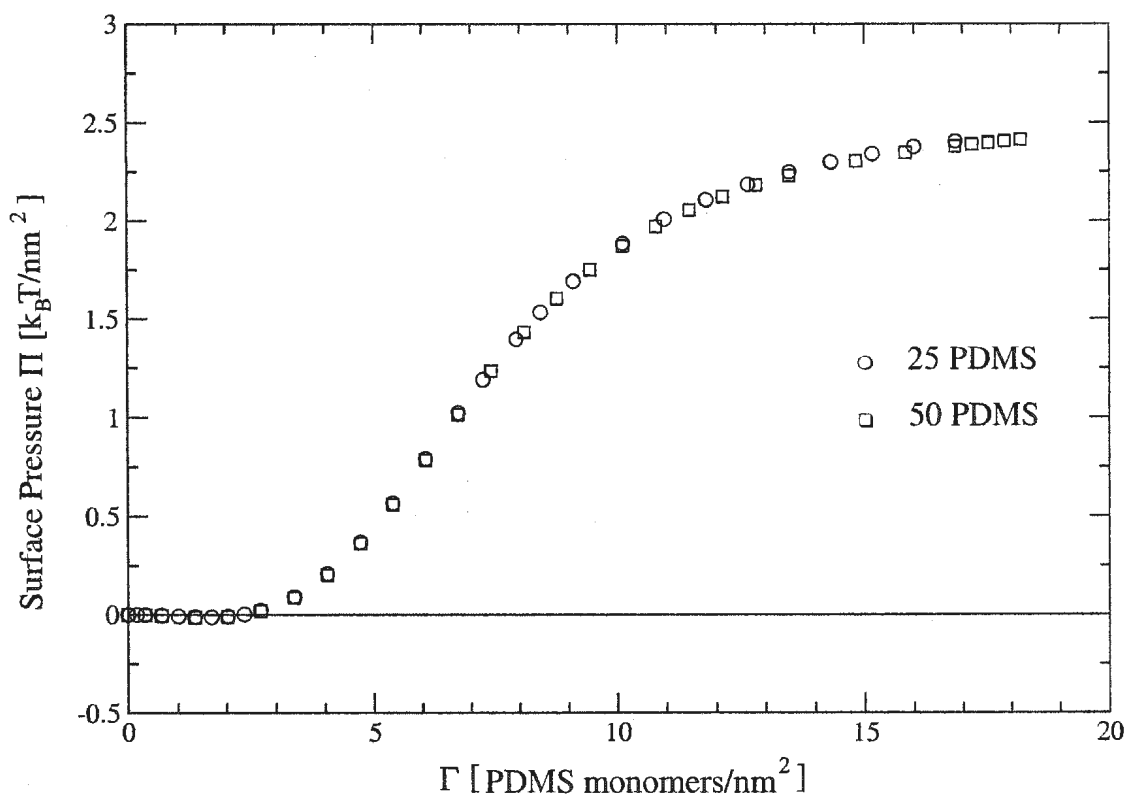


Figure 3.2: Surface pressure  $\pi$  as a function of the number of adsorbed monomers per unit area for PDMS homopolymers with  $M_w = 25,000$  and  $M_w = 50,000$ .

independent of the molecular weight of the homopolymer. For low coverages the surface pressure is zero except for very low  $\Gamma_A$ . It increases with  $\Gamma_A$ , reaching the plateau region at  $\Gamma_A \simeq 15$  monomers/nm<sup>2</sup>.

The leveling off of the surface pressure at higher coverages occurs at a maximum value in the surface concentration for which all chains in the system are highly extended into the solution. However, as Figure 3.3 shows, the density profiles exhibit a qualitative change at about this level of coverage,  $\Gamma = 10$ . This figure shows the density profiles for six values of  $\Sigma$  for the 25 PDMS homopolymer. It is obvious that at very low concentrations, the maximum density coverage at the surface is relatively very low but the thickness of the profile is on the order of the attractive well, i.e., 1

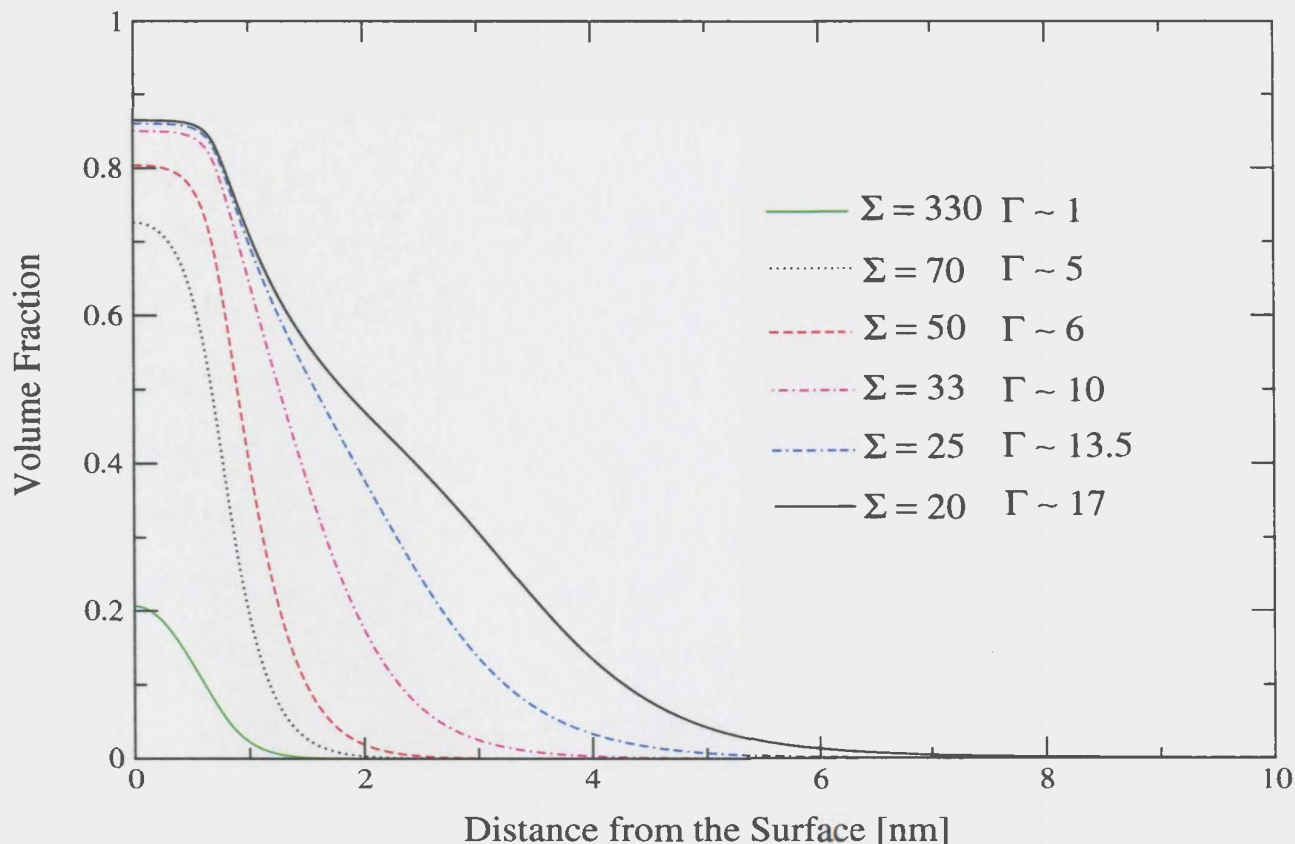


Figure 3.3: Density profiles for PDMS homopolymer with  $M_w = 25,000$  for different values of the surface coverages. The surface coverage,  $\Sigma$ , is expressed in units of  $\text{nm}^2$ , and the adsorbed amount  $\Gamma$  in numbers of adsorbed monomers per  $\text{nm}^2$

nm. Increasing the coverage, i.e., as  $\Sigma$  decreases, the thickness of the profile remains almost constant but the average density within the layer increases, since within this range of concentrations the adsorbed chains are not forced to extend away of the surface. Beyond  $\Sigma \lesssim 50 \text{ nm}^2$ , the maximum density saturates and the thickness of the layer begins to increase. The leveling off of the surface pressure occurs for concentrations greater than a full monolayer, in which cases a significant fraction of the polymer falls beyond the attractive well. This behavior of density profiles in addition to the leveling off of the surface pressure is in a good agreement with the experimental

observations of Kent *et al.* [8,12]. At full monolayer coverage,  $\Sigma \gtrsim 33 \text{ nm}^2$ , most of polymer chains are located in a region on the order of 1 nm from the adsorbed surface.

As mentioned earlier, one of the goals of the current work was to examine the effect of  $a_1$ , the location of the end of adsorbed block, in Baranowski's calculations. For systems of low coverage, all the  $A$ -blocks are located within a width of 1 nm consistent with results of Kent's experiments. Increasing the surface concentrations of the polymer system leads to thicker layer. Beyond a full monolayer coverage, the thickness of the layer becomes greater than the width of the region where the chain ends were assumed to start. This means that the  $A$ -block is being stretched. The onset of this stretching coincided approximately with the onset of the steep rise in the surface pressure. In principle, therefore, this could have been the cause of this increase. In order to test for this, different choices for  $a_1$  were used. This parameter affects the initial conditions for the propagators used to calculate the volume fraction for the  $A$  block. Choosing different values for  $a_1$  changes the initial conditions. However, the density profiles for all copolymers studied did not change. This indicates that the density profiles are not sensitive to  $a_1$ . In these systems, the monolayer is filled out at high coverage, and beyond this concentration, the free ends of the chains start to extend into the solution.

In summary, it has been found that the surface pressure isotherms for homopolymer adsorbed at the air-liquid interface depend on the total number of adsorbed monomers per unit area,  $\Gamma$ , and are independent of the molecular weight of the adsorbed chains, at least for relatively high molecular weights.

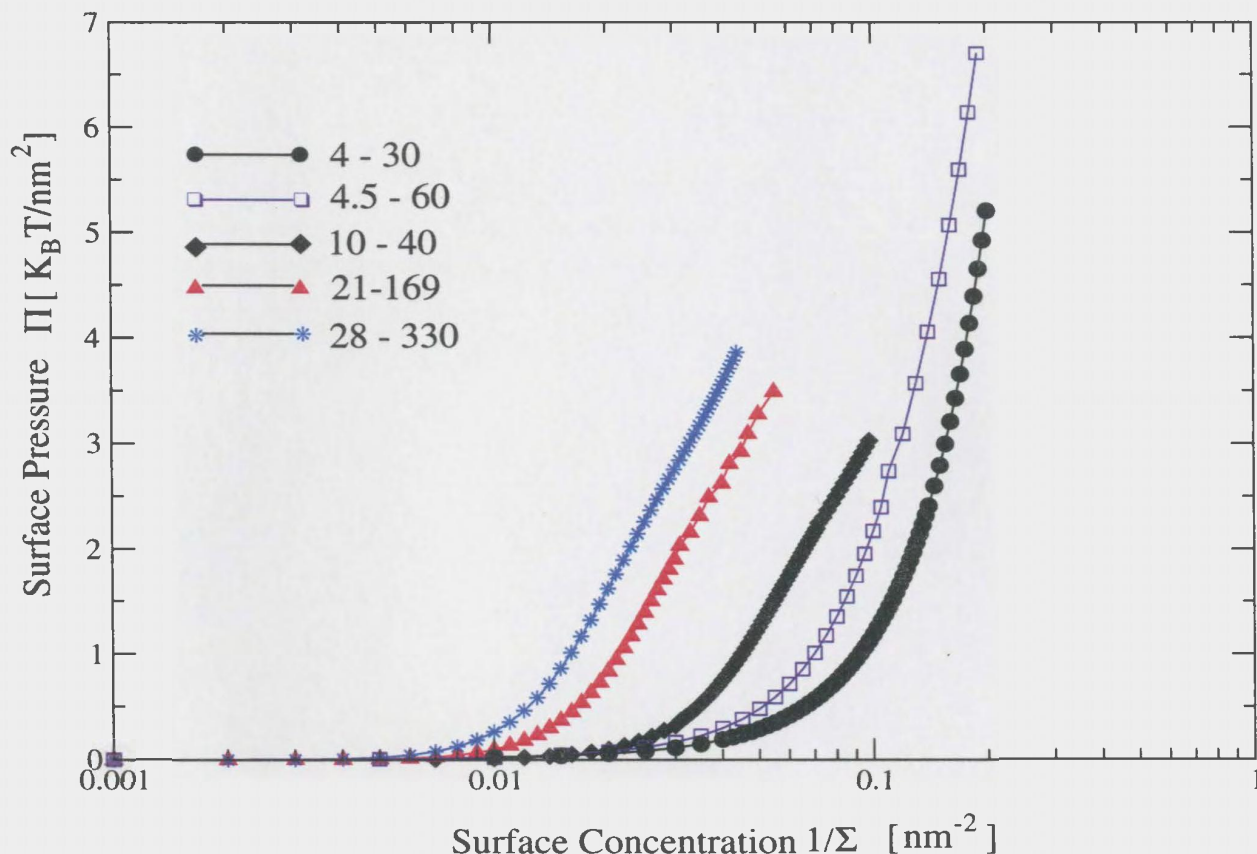


Figure 3.4: Surface pressure  $\pi$  as a function of the surface concentration,  $1/\Sigma$ . The polymers are labeled by the block molecular weights in kg/mol, of the PDMS and PS blocks, respectively.

### 3.3.2 Surface Pressure Isotherms - Copolymer

In this section the lateral compression of diblock copolymer/solvent system relevant to the experiments of Kent *et al.* [8, 12] is presented, analyzed and compared to later work done by Bijsterbosch *et al.* [11]. In addition, the numerical results of this thesis are compared to previous theoretical work [72] done to investigate Kent's experiments. Numerical calculations of the surface pressure isotherms as a function of surface concentration were performed for PDMS-PS copolymers used in Kent's experiments. The degrees of polymerization of each block are listed in table (3.1).

In Figure 3.4, the calculated surface pressure isotherms are shown as a function of

Copolymer $M_w$	4-30	4.5-60	10-40	21-169	25-35	28-330
$Z_A$	54	61	135	283	337	378
$Z_B$	288	576	384	1623	336	3169

Table 3.1: Polymers used in the calculations. The polymers are labeled by the block molecular weights, in kg/mol, of the PDMS and PS blocks respectively.

surface concentrations for the diblock copolymers. In each curve,  $\pi$  varies slowly for small coverages and increases smoothly for higher coverages with no rapid increase or steep rise such as what occurred in the results of Baranowski [72].

To compare the surface pressure isotherms for the diblock copolymer with that for the homopolymer, it is useful to express the surface pressure as function of the surface concentration of PDMS-monomers. This comparison is presented in Figure 3.5. For the 25-35 PDMS-PS copolymer,  $Z_A \simeq Z_B$  and so the isotherm falls very close to the homopolymer curve. This can be interpreted as meaning real surface pressure is mainly due to the interactions among the  $A$  chains, and the contribution from the dangling  $B$ -block is negligible up to the surface concentration,  $\Gamma \simeq 12$  PDMS monomers/nm<sup>2</sup>, where the deviation from the homopolymer isotherm begins. A remarkable note from Figure 3.5, is that for 28-330, 21-169, 10-40 PDMS-PS copolymers, the isotherms almost coincide with each other.

### 3.4 Surface Pressure Excess

From Figure 3.5, the surface pressure excess,  $\Delta\pi$ , for each copolymer can be calculated as the difference between the copolymer and homopolymer pressures at each  $\Gamma_A$ . The results for each curve can then be converted to functions of  $\Sigma$ , and this surface pressure

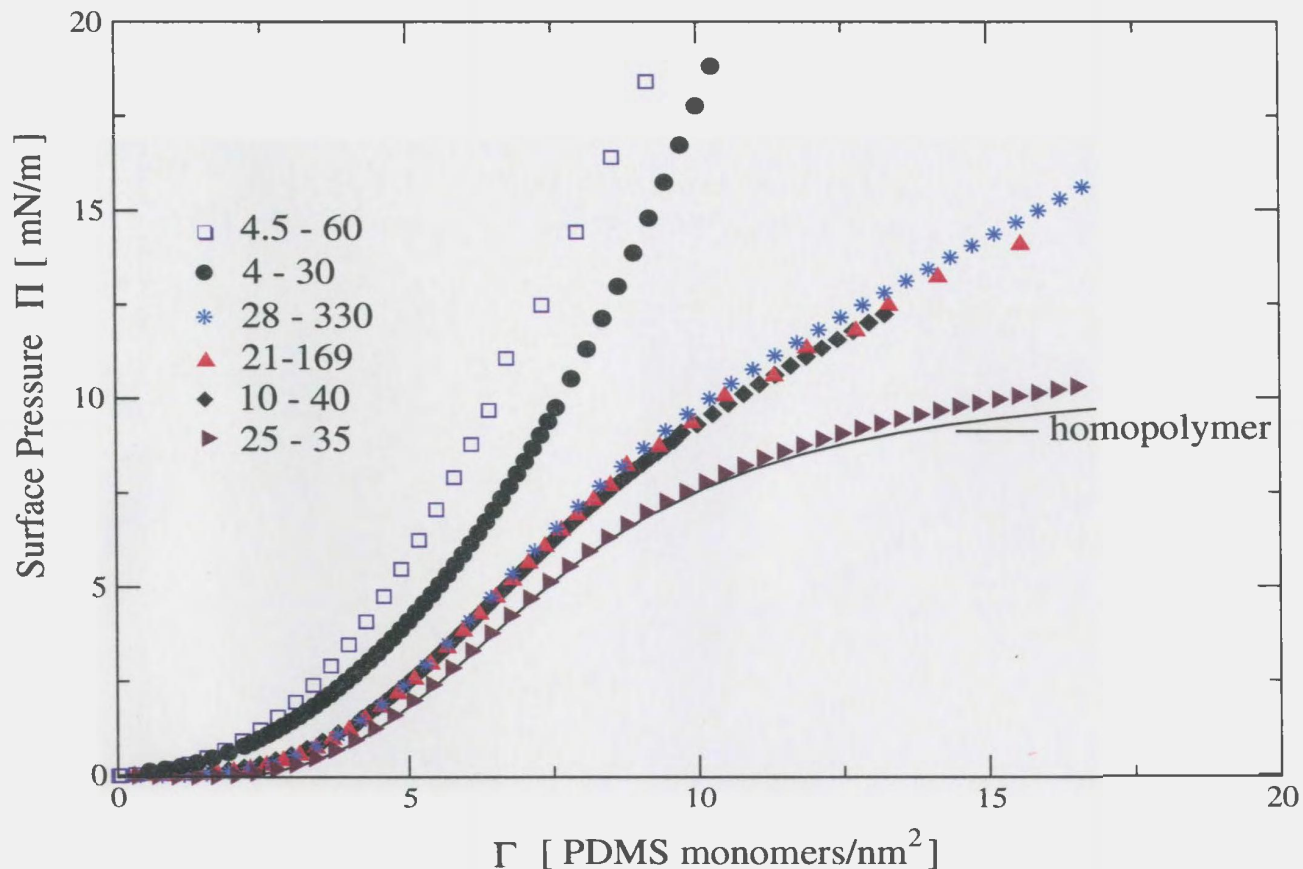


Figure 3.5: Comparison of surface pressure,  $\pi$  as a function of the adsorbed PDMS monomers, for the diblock copolymer with homopolymer. The polymers are labeled by the block molecular weights in kg/mol, of the PDMS and PS blocks, respectively.  $T=300K$  as the ambient temperature was used to express the pressure in the units of [mN/m].

excess, which is due to the dangling PS blocks, is given by

$$\Delta\pi \equiv \pi^C(\Gamma_A) - \pi^H(\Gamma_A) \quad . \quad (3.48)$$

The results are shown in Figure 3.6.

In Figure 3.6, it appears that the surface pressure excess,  $\Delta\pi$ , increases smoothly as a function of the number of chains per unit area,  $1/\Sigma$ , and there is again no rapid increase at high coverage. Qualitatively, this agrees with the aSCF and scaling

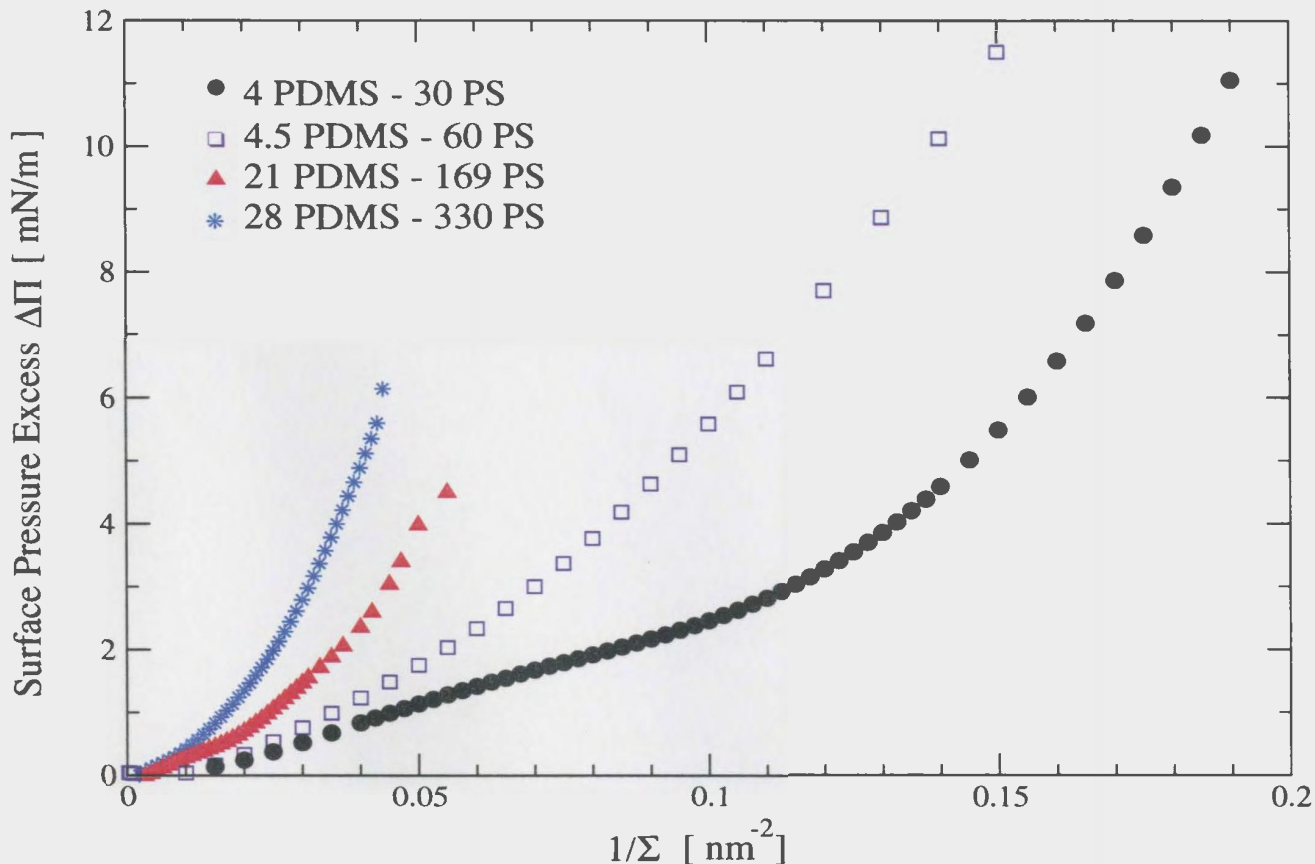


Figure 3.6: Surface pressure excess,  $\Delta\pi$ , as a function of the number of chains per unit area  $1/\Sigma$ .

theories. To make a quantitative comparison, the results of Fig. 3.6 are plotted on a double-logarithmic plot, Fig. 3.7. All curves have the same overall behavior.

Except at very low densities, each set of results falls approximately on a straight line, which indicates a power law behavior. The fitted powers are shown on the Figure. They all range from about 1.5 to 1.8, quite close to the aSCF values of  $5/3$ . The deviation from power law behavior at low coverage may be an artifact due to the subtraction of two small values of surface pressure, or a real effect reflecting the very low polymer density.

These powers are much smaller than those obtained in the experimental studies of Kent *et al.* [12]. They reported that the excess surface pressure still scales as a

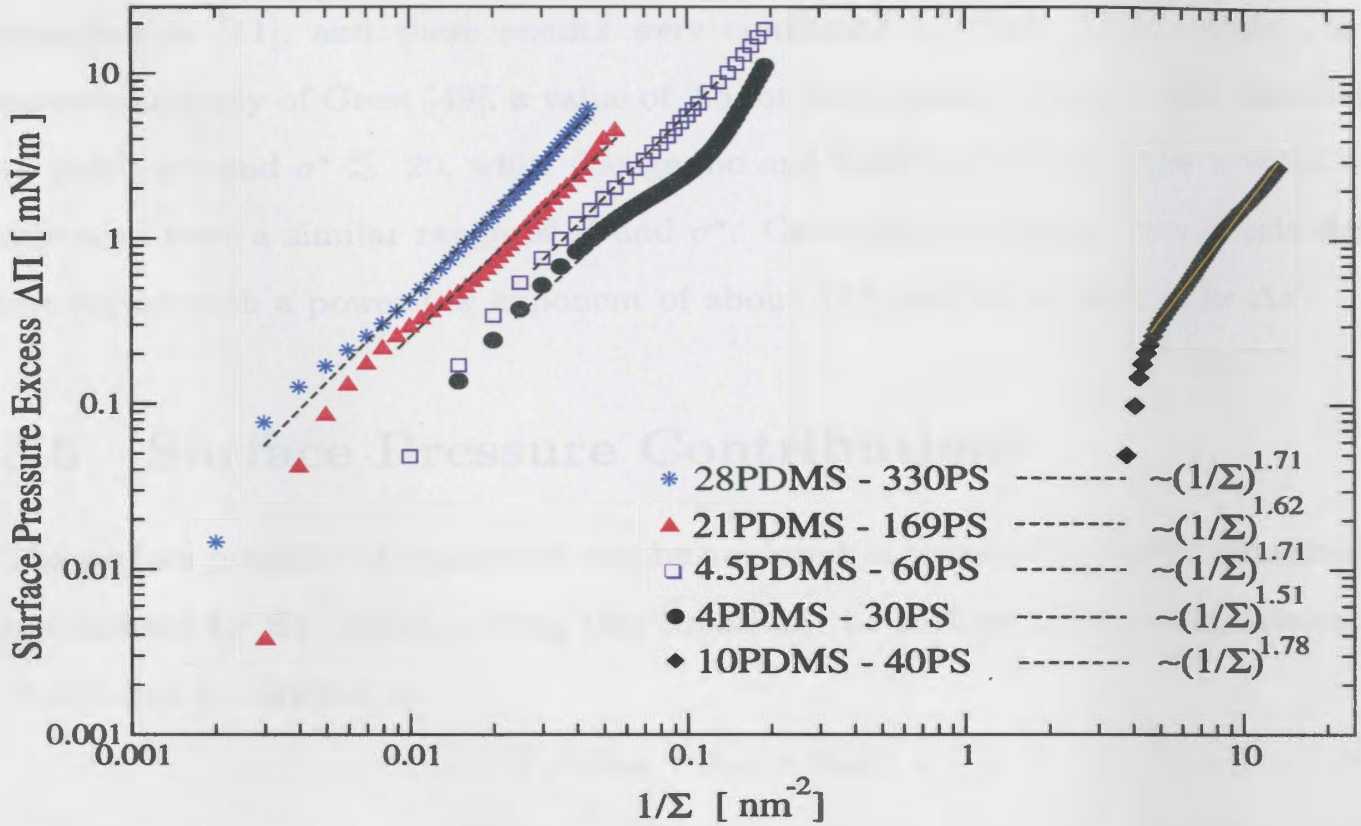


Figure 3.7: Surface pressure excess,  $\Delta\pi$ , as a function of the number of chains per unit area  $1/\Sigma$ , on a double-logarithmic scale for different copolymers. The dashed line is the line of the best fit using an assumed exponent power law dependence.

power law with exponent ranges from approximately 4.2 to 6.6. As shown in Fig. 1.3, Baranowski's nSCF study reported two regions for  $\Delta\pi$  [72]. At low coverage,  $\Delta\pi$  obeyed a power law with an exponent of  $5/3$ , while at higher coverage, the exponents ranged between 5.3 to 7.2. These results were in semi-quantitative agreement with Kent's experiments. Our new results can be compared directly with Baranowski's by comparing Fig. 3.7 with Fig. 1.3. For each polymer, we find only one regime with a power of about  $5/3$ . Other theoretical and experimental studies also found only small powers. Currie *et al.* [60] reported a scaling exponent of  $5/3$  for Bijsterbosch's

experiments [11], and these results were confirmed by their nSCF study. In the numerical study of Grest [49], a value of 2.5 for the exponent of  $\Delta\pi$ , was obtained for all polymers and  $\sigma^* \lesssim 20$ , while Carignano and Szleifer [47] obtained a value of 2.4 exponent over a similar range of  $Z$  and  $\sigma^*$ . Calculations used in this thesis showed one region with a power law exponent of about 5/3, and no rapid rise in  $\Delta\pi$ .

### 3.5 Surface Pressure Contributions

The surface pressure of copolymer can be analyzed in terms of the three contributions represented by Eq. (3.43). Using this equation, the surface pressure expression, Eq. (3.40), can be written as

$$\pi = \pi_{ext} + \pi_{int} + \pi_{ent} \quad , \quad (3.49)$$

where each term corresponds to a contribution to the  $\mathcal{L}$  in Eqs. (3.42) and (3.43), and has the corresponding physical interpretation.

In Figure 3.8 the contribution  $\pi_{ext}$  as a function of  $\Gamma_A$  is presented. All the curves are nearly identical and the same as for the homopolymer. Hence, the external interactions have very little effect on the excess surface pressure of the copolymers. Figure 3.9 shows the contribution due to the interactions between all components in the system. The homopolymer isotherm shows quadratic behavior in the range  $6 \leq \Gamma \leq 8$ , while it increases linearly for the positive values. For the 10-40, 21-169, and 28-330 PDMS-PS copolymers, there is a plateau in the range  $6 \leq \Gamma \leq 8$ . The 4.5-60 and 4-30 PDMS-PS copolymers do not have a plateau and a negative contribution to the surface pressure still exists for high surface coverages for those copolymers. Figure 3.10 shows  $\pi_{ent}$ , the entropic contribution to the surface pressure. The dominant factors that control all the curves in this figure are the size of the anchored  $A$ -block and the asymmetry ratio. It is obvious from Figure 3.10 that the isotherms of 10-40,

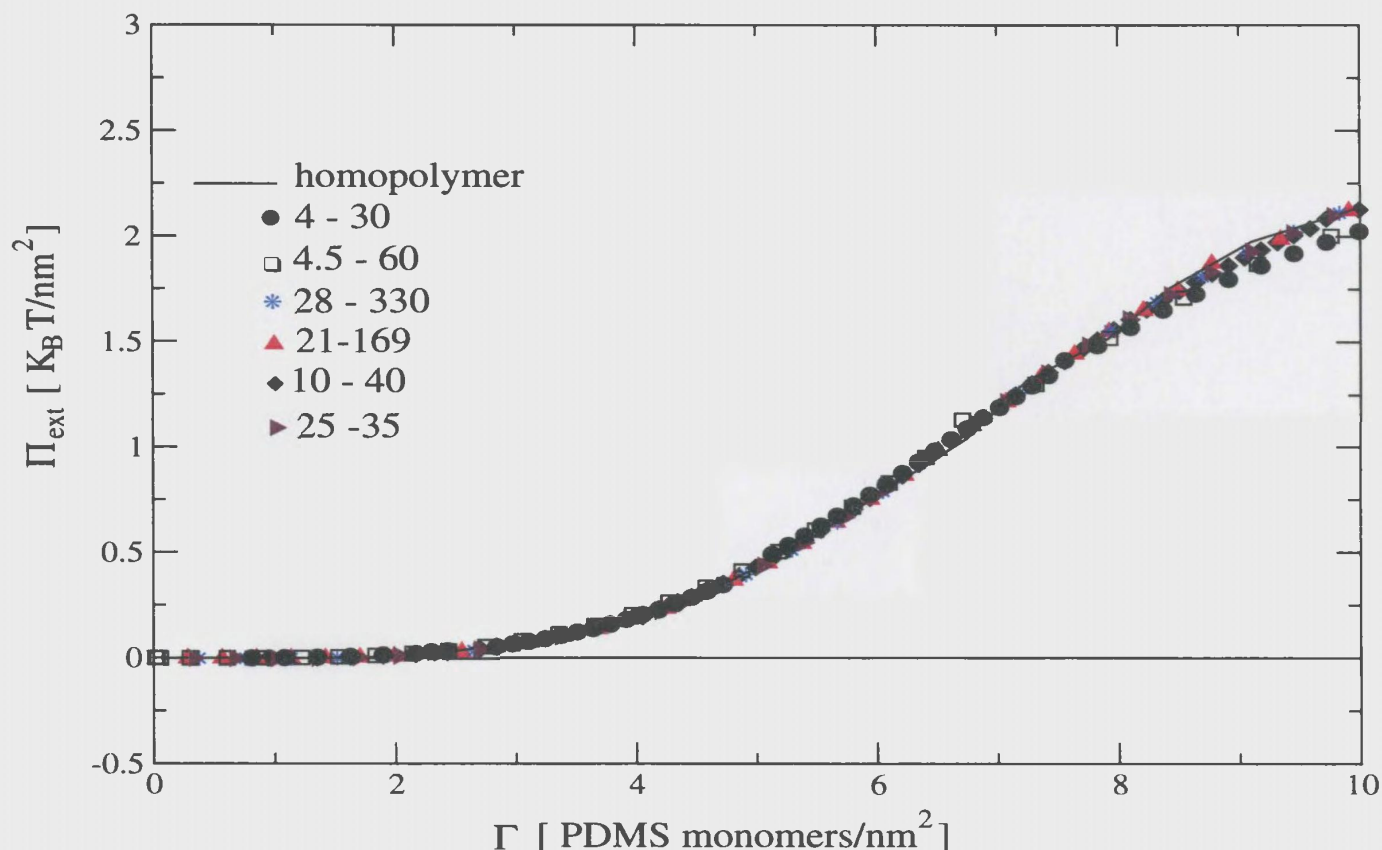


Figure 3.8: The contribution  $\pi_{ext}$  to the surface pressure  $\pi$  as a function of the number of PDMS monomers per unit area adsorbed onto the surface.

21-169, and 28-330 PDMS-PS copolymers have a local maximum at  $\Gamma = 6$ , while 4-30 and 4.5-60 PDMS-PS copolymer isotherms increase faster as a function  $\Gamma$ . It is obvious that the 25-35 PDMS-PS copolymer has a negative values for  $\Gamma > 8$ .

### 3.6 Comparison with Earlier nSCF Calculations

In his study of lateral compression of polymer layers, Baranowski [72] used nSCF theory to calculate the surface pressure excess,  $\Delta\pi$ , for copolymers investigated by Kent and coworkers. First a homopolymer/solvent system was studied. He found the surface pressure as a function of surface coverages, then he modeled the diblock

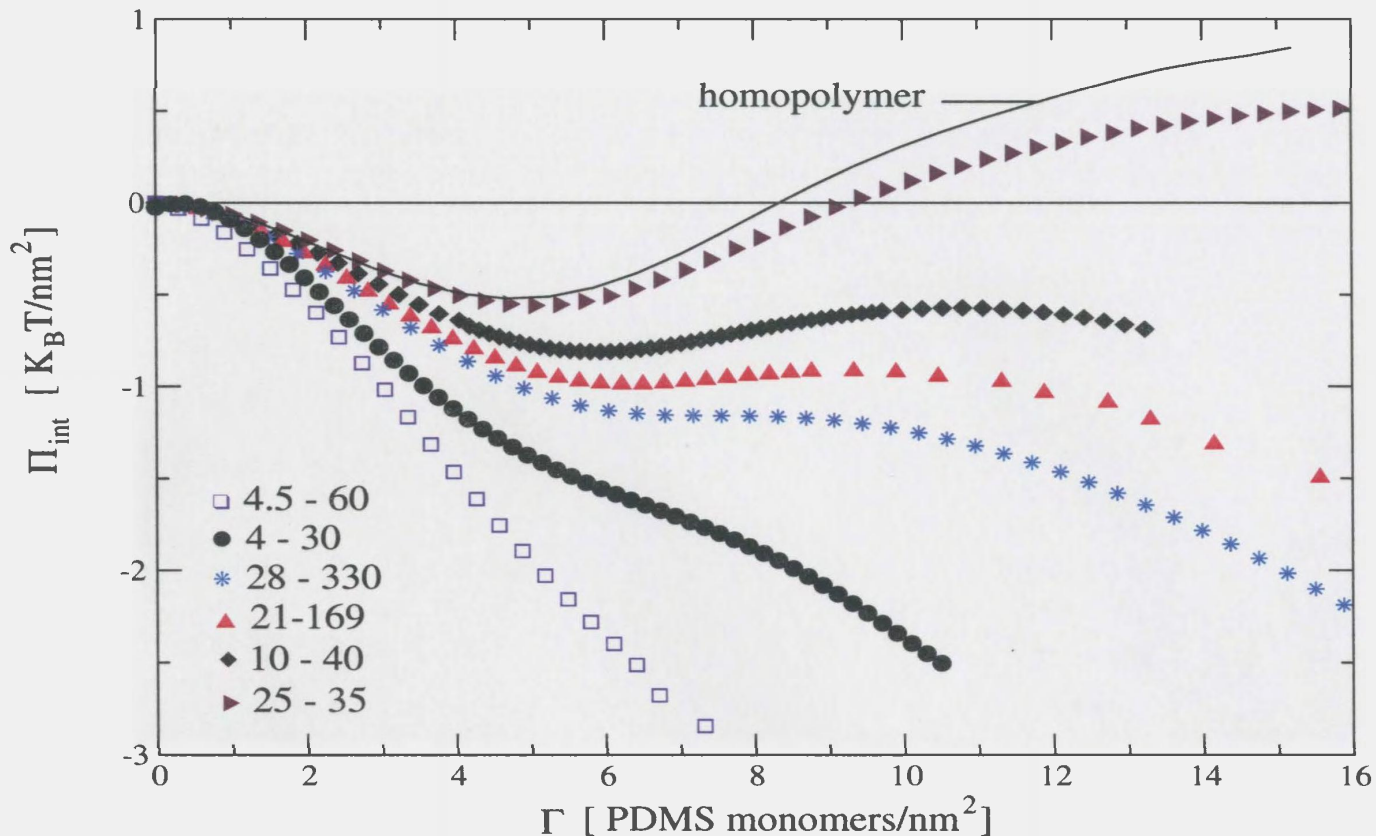


Figure 3.9: The contribution  $\pi_{int}$  to the surface pressure  $\pi$  as a function of the number of PDMS monomers per unit area adsorbed onto the surface.

copolymer/solvent systems. Then, he found  $\Delta\pi$ . He found a semi-quantitative agreement with values obtained in Kent's experiments. Baranowski found that for the entropic contribution, the surface pressure isotherms have a steep raise at high coverages except for the 25-35 PDMS-PS copolymer isotherm which has a similar behavior like the homopolymer.

In this thesis, nSCF calculations were made to study the systems investigated by Kent *et al.* using the same procedure followed by Baranowski. No rapid rise in  $\Delta\pi$  was found. The surface pressure isotherms showed only one region with  $\Delta\pi \sim \sigma^{5/3}$  as predicted by aSCF theory.

To analyze these results, in order to find the reason for this deviation from Bara-

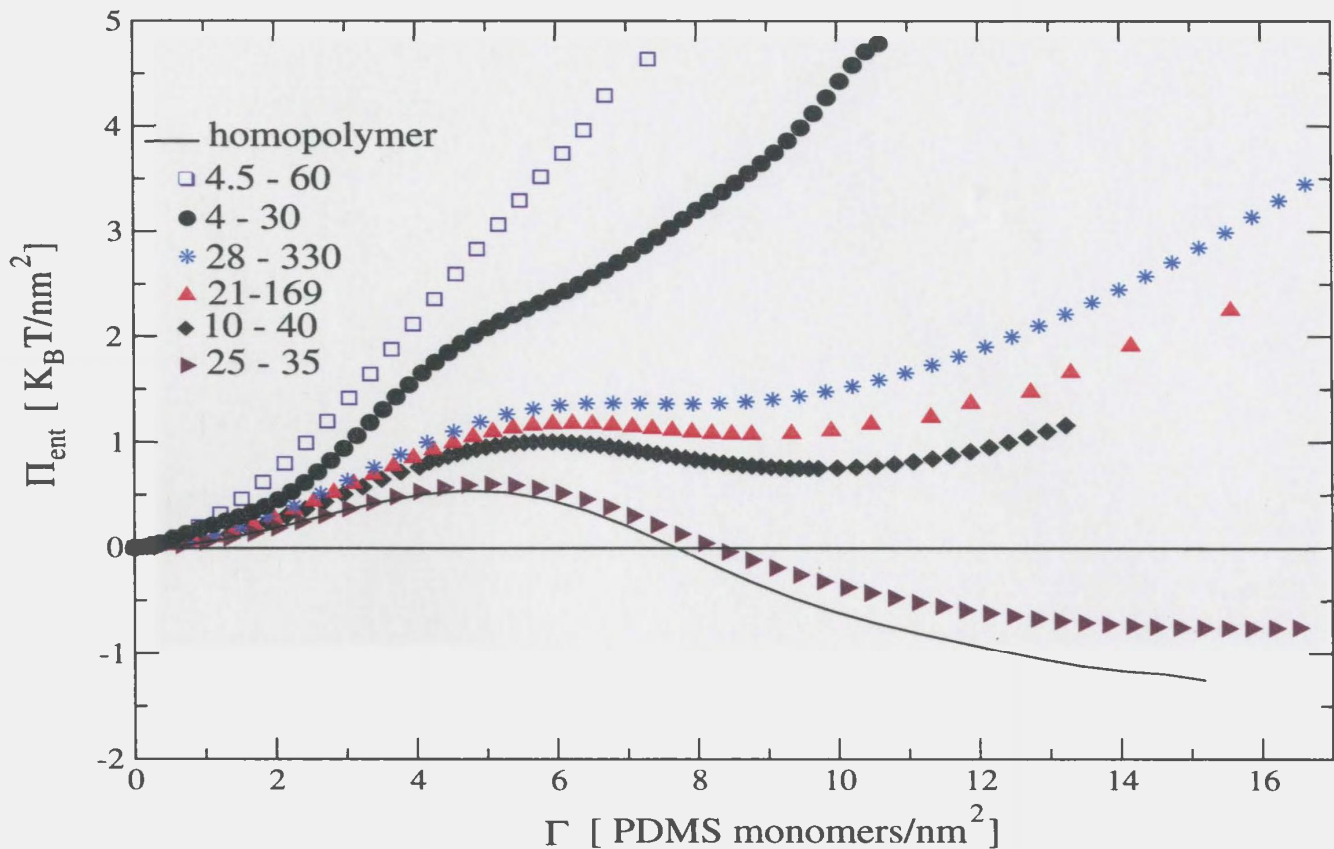


Figure 3.10: The contribution  $\pi_{ent}$  to the surface pressure  $\pi$  as a function of the number of PDMS monomers per unit area adsorbed onto the surface.

nowski's work, we first examined different values of  $a_1$  as described in section 3.2.5. Almost the same surface pressures  $\pi$ , for all values of  $a_1$ , were obtained. This is an indication that this is not the reason for this deviation. In the course of the work, the computer code were extensively re-examined, and no errors were found. We probed the effect of  $L$ , which is the separation of the two surfaces in the calculations. There is only one surface in the experiments, so  $L$  needs to be large enough that it has no effect on the calculations. It was discovered that the rapid increase in  $\Delta\pi$  obtained by Baranowski was probably a result of choosing  $L$  to be too small. The author of this thesis found that, when  $L$  is small enough to perturb the tethered layers, the effect is to cause a sudden increase in  $\Delta\pi$  as reported by Baranowski and shown in

Fig 1.3. The transition from region of weak dependence on  $\Sigma$  to strong dependence occurs when the polymer begins to encounter this second surface.

# Chapter 4

## Concluding Remarks

To investigate the physical and structural properties of polymer/solvent systems near surfaces and interfaces, numerical self-consistent field calculations were performed. Moreover, results obtained in this thesis were compared to other experimental and theoretical studies found in the literature [7, 8, 11, 12, 60, 72, 102]. A major focus was on understanding the density profiles and the surface pressure isotherms for both homopolymer and copolymer systems. Results obtained by nSCF theory were compared to these predicted by aSCF models for the surface pressure excess. This chapter summarizes and concludes the work performed in this thesis.

### 4.1 Summary of the Results

A key issue in the brush models is the monomer density profile, which is a study of the variation of the density as a function of the distance from the surface. To give a quantitative description of these profiles, polymer configurations are idealized as space curves and the partition function is written as a functional integral over the range of the configuration space. The introduction of the concept of incompressibility as

well as the mean field approximation eliminates the fluctuations in the local volume fractions and results in a set of coupled equations for the density profiles of every component, self-consistent potentials and a free energy expression written in terms of the densities and interaction parameters.

In chapter 3, the lateral compression of homopolymer and copolymers at the air-liquid interface is studied. In various solution conditions, Kent *et al.* [7, 8, 12, 102], probed diblock copolymer monolayers, in which the adsorption from solution of PDMS in good solvents at the air-liquid interface was explored. They determined the density profile as a function of the surface density, the molecular weights of PS and PDMS blocks, and the solution conditions. They reported a disagreement with analytical profile forms and scaling prediction, in addition to a deviation from the predicted surface pressure power law. They noted a rapid increase in the surface pressure excess as a function of grafted chains per unit area. In their investigations, they found that the strong-stretching limit assumed by the aSCF calculations and scaling theories is not valid over this  $\sigma^*$  range [20]. By contrast, Currie *et al.* [60] found a semi-quantitative agreement between nSCF calculations and experimental surface pressure isotherms of PS-PEO diblock copolymers at the air-water interface measured by Bijsterbosch *et al.* [11]. In these theoretical studies they found that the scaling relations are corroborated experimentally for long PEO-chains, provided that contributions to  $\pi$  arising from the PEO adsorption at the air-water interface are taken into account. No sudden increase in the surface pressure was reported and the pressure isotherms were increasing smoothly as a function of the grafted chains per unit area.

In a nSCF study performed by Pépin and Whitmore [111], they found that the brush height scales as  $h_{rms} \sim Z^{0.86} \sigma^{0.27}$ , in good agreement with the thickness of the brush layer concluded by Kent *et al.*, which scales approximately as  $h \sim Z^{0.86} \sigma^{0.22}$ .

These values are consistent with a previous nSCF ones of  $h^{0.81}\sigma^{0.24}$  [39].

Moreover, another prediction made by the single-chain mean-field theory (SCMF) [50] for the height of the brush is in very good agreement with the Kent's experiments for all surface coverages. Their predictions for the brush thickness scales as  $h \propto Z^{0.9}\sigma^{0.25}$ .

The analytic pictures predict that the surface pressure for asymmetric copolymers should scale as  $(1/\Sigma)^{5/3}$ , the result which is confirmed by nSCF calculations performed in this thesis and by Currie *et al.* [60], in which the surface pressure increases smoothly as a function of the chains per unit area and no sharp pressure isotherms were predicted. The SCMF model obtained similar results, agreeing with Kent's results for the surface pressure excess up to values of surface coverages of  $\sigma^* \simeq 8$ . The reason for the deviations at higher coverage may arise from the way of investigating the power law dependencies of the surface pressure and brush height, as explained by Currie *et al.* [60]. Alternatively, Carignano and Szleifer suggested that these deviations are due to non-equilibrium effects, [47].

Another problem is the determination of the adsorbed amount of polymer on the surface. Bijsterbosch *et al.* [11], deposited the PS-PEO block copolymer on the air-water interface using chloroform as a solute. The deposited amount can be determined with a reasonable accuracy, since both chloroform and PS are highly hydrophobic and they do not mix with water.

Kent *et al.* used either a polymer solution, which had a density higher than the organic bulk phase, or dry block copolymer [12,102]. The polymer density is not directly known during the experiment, due to loss of polymer during deposition, so the density was determined via integration of the neutron reflectivity curves. This is inaccurate, especially at low polymeric densities [60]. This inaccuracy is important in measuring the surface pressure or layer thickness.

From nSCF calculations done in this thesis, we found that there is no rapid increase in the surface pressure excess,  $\Delta\pi$ , as a function of the surface coverage. Instead, the density dependence scaled as  $\Delta\pi \sim \sigma^{5/3}$ , which is compatible with results predicted by aSCF theory. By testing different values for the width of the interface, we found that the density profiles for the PDMS homopolymer did not change. On the other hand, decreasing the linear dimension of the system results in increasing the excess surface pressure. This is the probable reason for the results obtained by Baranowski [72].

## 4.2 Future Work

End-tethered polymers need more extensive work, experimentally as well as theoretically. Physical behavior of these systems needs more investigation in order to give an exact description for the surface pressure excess, in addition to subtle determination of brush height for highly stretched polymer chains. The SCF theory used in this thesis can be extended to include lateral fluctuations. Do we get a quantitative explanation if we include these fluctuations in the surface pressure calculations? How can we be certain if the systems, under investigation, reached the equilibrium? Moreover, it should be emphasized that, considering polymer systems near surfaces to be in one dimension is a simplification. This leads to attempt to study these systems near surfaces in two or three dimension.

Complicated polymer systems under the influence of several factors, which affect the interactions among the constitutions of these systems, should be considered.

# Bibliography

- [1] J.M. G. Cowie, *Polymers: Chemistry & Physics of Modern Materials*, (2nd edition, Blackie and Son limited, England, 1991), pp. 1-23.
- [2] J.N. Israelachvili, M. Tirrell, J. Klein, and Y. Almog, *Macromolecules* **17**, 204 (1984).
- [3] L.T. Lee, O. Guiselin, B. Farnoux, and A. Lapp, *Macromolecules* **24**, 2518 (1991).
- [4] P. Auroy, L. Auvray, and L. Léger, *Physical Review Letters* **66**, 719 (1991).
- [5] O. Guiselin, L.T. Lee, B. Farnoux, and A. Lapp, *J. Chem. Phys.* **95**, 4632 (1991).
- [6] P. Auroy, L. Auvray, and L. Leger, *Macromolecules* **24**, 2523 (1991).
- [7] M.S. Kent, L. Bosio, and F. Rondelez, *Macromolecules* **25**, 6231 (1992).
- [8] M.S. Kent, L.T. Lee, B. Farnoux, and F. Rondelez, *Macromolecules* **25**, 6240 (1992).
- [9] J.B. Field, C. Toprakcioglu, R. C. Ball, H. B. Stanley, L. Dai, W. Barford, J. Penfold, G. Smith, and W. Hamilton *Macromolecules* **25**, 434 (1992).

- [10] H. Watanabe, M. Tirrel, *Macromolecules* **26**, 6455 (1993).
- [11] H.D. Bijsterbosch, V.O. de Haan, A.W. de Graaf, M. Mellema, F. Leermakers, M. Cohen Stuart, and A. van Well *Langmuir* **11**, 4467 (1995).
- [12] M.S. Kent, L.T. Lee, F. Rondelez, and G.S. Smith *J. Chem. Phys.* **103**, 2320 (1995).
- [13] M.S. Kent, B. Factor, S. Satija, P. Gallagher, and G. Smith *Macromolecules* **29**, 2843 (1996).
- [14] E.S. Pagac, D. Prieve, Y. Solomentsev, and R. Tilton *et al.*, *Langmuir* **13**, 2993 (1997).
- [15] M.S. Kent, J. Majewski, G. Smith, L.T. Lee, and S. Satija *J. Chem. Phys.* **108**, 5635 (1998).
- [16] O. Prucker and J. R uhe, *Macromolecules* **31**, 592 (1998).
- [17] O. Prucker and J. R uhe, *Macromolecules* **31**, 602 (1998).
- [18] H.D. Bijsterbosch, M. Stuart, G. Fler, P. van Caeter, and E. Goethals, *Macromolecules* **31**, 7436 (1998).
- [19] M.G. Mu oz, F. Monroy, F. Ortega, R. Rubio, and D. Langevin *Langmuir* **16**, 1083 (2000).
- [20] M.S. Kent, *Macromol. Rapid Commun.* **21**, 243 (2000).
- [21] C. Luap and W.A. Goedel, *Macromolecules* **34**, 1343 (2001).
- [22] W.A. Goedel, P. Eibeck, and H. Xu, *Macromolecules* **35**, 801 (2002).
- [23] M. Baum and W. J. Brittain, *Macromolecules* **35**, 610 (2002).

- [24] P.J. Yoo, K.Y. Suh, and H.H. Lee, *Macromolecules* **35**, 3205 (2002).
- [25] K.N. Jayachandran, A. Takacs-Cox, and D. E. Brooks, *Macromolecules* **35**, 4247 (2002).
- [26] P.-G. de Gennes, *Macromolecules* **14**, 1637 (1981).
- [27] P.-G. de Gennes, *Scaling concepts in polymer physics*, (Cornell University Press, Ithaca, NY, 1979).
- [28] E.P. K. Currie, *Brushes and Soap: Grafted Polymers and their Interactions with Nanocollides*, Ph.D thesis, Wageningen University (2000).
- [29] H. Yamakaw, *Modern Solvent Theory of Polymer Solutions*, (Harper & Row, New York) (1971).
- [30] P.-G. de Gennes, *Macromolecules* **13**, 1069 (1980).
- [31] K. M.Hong and J. Noolandi, *Macromolecules* **14**, 727 (1981).
- [32] P.-G. de Gennes, *Macromolecules* **14**, 1637 (1981).
- [33] P.-G. de Gennes, *Macromolecules* **15**, 492 (1982).
- [34] J. Scheutjens and G. J. Fleer, *Macromolecules* **18**, 1882 (1985).
- [35] M. Murat and G. S. Grest, *Macromolecules* **22**, 4054 (1989).
- [36] C.M. Marques and J. F. Joanny, *Macromolecules* **22**, 1454 (1989)
- [37] E.B. Zhulina, O. Borisov, and V. Priamitsyn *Journal of Colloid and Interface Science* **137**, 495 (1990).
- [38] C.M. Wijmans and J. Scheutjens *Macromolecules* **25**, 2657 (1992).

- [39] R. Baranowski and M.D. Whitmore, *J. Chem. Phys.* **103**, 2343 (1995).
- [40] M.D. Whitmore and J. Noolandi, *Macromolecules* **21**, 1482 (1988).
- [41] S.T. Milner, T.A. Witten, and M.E. Cates, *Macromolecules* **21**, 2610 (1988).
- [42] C.M. Marques and J.F. Joanny, *Macromolecules* **23**, 268 (1990).
- [43] M.D. Whitmore and J. Noolandi, *Macromolecules* **23**, 3321 (1990).
- [44] O.A. Evers, J. Scheutjens, and G.J. Fleer, *Macromolecules* **23**, 5221 (1990).
- [45] J.D. Vavasour and M.D. Whitmore, *Macromolecules* **26**, 7070 (1993).
- [46] A. Chakrabarti, P. Nelson, and R. Toral, *J. Chem. Phys.* **100**, 748 (1994).
- [47] M.A. Carignano and L. Szleifer, *J. Chem. Phys.* **100**, 3210 (1994).
- [48] J.F. Marko, A. Johner, and C.M. Marques, *J. Chem. Phys.* **99**, 8142 (1993).
- [49] G.S. Grest, *Macromolecules* **27**, 418 (1994).
- [50] M.A. Carignano and L. Szleifer, *Macromolecules* **28**, 3197 (1995).
- [51] A.N. Semenov, J. Bonet-Avlos, A. Johner, and J.F. Joanny, *Macromolecules* **29**, 2179 (1996).
- [52] M. Aubouy, O. Guiselin, and E. Raphaël, *Macromolecules* **29**, 7261 (1996).
- [53] T.C. Clancy and S.E. Webber, *Macromolecules* **30**, 1340 (1997).
- [54] M. Guenza and K.S. Schweizer, *Macromolecules* **30**, 4205 (1997).
- [55] R. Hasegawa and M. Doi, *Macromolecules* **30**, 3086 (1997).
- [56] J. Klein and G. Rossi, *Macromolecules* **31**, 1979 (1998).

- [57] R.R. Netz and M. Schick, *Macromolecules* **31**, 5105 (1998).
- [58] J.M. Méndez-Alcaraz, A. Johner, and J.F. Joanny, *Macromolecules* **31**, 8297 (1998).
- [59] R. Baranowski and M. D. Whitmore, *J. Chem. Phys.* **108**, 9885 (1998).
- [60] E.P.K. Currie, V.O. de Haan, A.W. de Graaf, M. Mellema, F.A.M. Leermakeres, M.A. Cohen Stuart, and A.A. van Well, *Macromolecules* **32**, 487 (1999).
- [61] G.J. Fleer, J. van Male, and A. Johner, *Macromolecules* **32**, 825 (1999).
- [62] G.J. Fleer, J. van Male, and A. Johner, *Macromolecules* **32**, 845 (1999).
- [63] J. Jimenez, J. de Joannis, I. Bitsanis, and R. Rajagopalan *Macromolecules* **33**, 8512 (2000).
- [64] J. des Cloizeaux, *Le Journal De Physique* **4**, 281 (1975).
- [65] J.D. Vavasour and M. D. Whitmore, *Macromolecules* **34**, 3471 (2001).
- [66] W. Nowicki, *Macromolecules* **35**, 1424 (2002).
- [67] J. van der Gucht, N. A. M. Besseling, and G. J. Fleer, *Macromolecules* **35**, 2810 (2002).
- [68] A.A. Mercurieva, T. Birshtein, E. Zhulina, P. Iakovlev, J. van Male, and F. Leermakers *Macromolecules* **35**, 4739 (2002).
- [69] M. Rangarajan, J. Jimenez, and R. Rajagopalan, *Macromolecules* **35**, 6020 (2002).
- [70] Nam-Kyung Lee, A. Johner, and T. A. Vilgis, *Macromolecules* **35**, 6043 (2002).

- [71] G. Fleer and J. Lyklema, *Adsorption from Solution at the Solid/Liquid Interfaces*, edited by G.D. Prafft and C.H. Rochester (Academic Press, London, 1983), pp. 156-219.
- [72] R. Baranowski, Ph.D. thesis, Memorial University of Newfoundland, (1998).
- [73] P.-G. de Gennes, *Advances in Colloid and Interface Science* **27**, 189 (1987).
- [74] P.-G. de Gennes and P. Pincus, *Journal de Physique Letters* **44**, L (1983).
- [75] E. Bouchaud and M. Daoud, *Journal de Physique* **48**, 1991 (1987).
- [76] C. Ligoure, *Journal de Physique II* **3**, 1607 (1993).
- [77] D. Williams, *Langmuir* **9**, 2215 (1993).
- [78] S. Alexander, *J. Phys. Fr.* **38**, 983 (1977).
- [79] S. Edwards, *Proc. Phys. Soc.* **85**, 613 (1966).
- [80] A.K. Dolan and S. Edwards, *Proc. R. Soc. Lond.* **A343**, 427 (1975).
- [81] A.N. Semenov and J.F. Joanny, *Europhys. Lett.* **29**, 279 (1995).
- [82] J.B. Avalos, J. Joanny, A. Johner, and A. Semenov *Europhys. Lett.* **35**, 97 (1996).
- [83] J. Scheutjens and G. J. Fleer, *J. Chem. Phys.* **83**, 1619 (1979).
- [84] J. Scheutjens and G. J. Fleer, *J. Chem. Phys.* **84**, 178 (1980).
- [85] G.J. Fleer, M. Stuart, J. Scheutjens, T. Cosgrove, and B. Vincent *Polymers at Interfaces* (Chapman Hall, London, 1993).
- [86] C. van der Linden, F. leermakers, and G.J. Fleer *Macromolecules* **29**, 1172 (1996).

- [87] S.T. Milner, T.A. Witten, and M.E.Cates, *Europhys. Lett.* **5**, 413 (1988).
- [88] V.A. Priamitsyn, O.V. Borisov, E.B. Zhulina, and T.M. Birshtein, *Modern Problems in Physical Chemistry of Solutions*, (Donish and Leningrad University, Dunshabe and Leningrad (USSR), 1987)
- [89] E.B. Zhulina, O.V. Borisov, and V.A. Priamitsyn, *Journal of Colloid and Interface Science* , **137**, 495 (1990).
- [90] S.T. Milner, *Journal of Polymer Science:Part B* **32**, 2743 (1994).
- [91] S.T. Milner, *J. Chem. Soc. Faraday Trans.* **86**, 1349 (1990).
- [92] J.I. Martin and Z.G. Wang, *J. Chem. Phys.* **99**, 2833 (1995).
- [93] D.F Shim and M. E Cates, *J. Phys. (Paris)* **51**, 701 (1990).
- [94] C.M. Marques, J.F. Joanny, and L. Leibler, *Macromolecules* **21**, 1051 (1988).
- [95] G. Hadziioannou, S. Patel, S.Granik, and M. Tirrel, *J. Am. Chem. Soc.* **108**, 2869 (1986).
- [96] S. Patel and G. Hadziioannou, *Colloids and Surfaces* **31**, 157 (1988).
- [97] J. Marra and M. L. Hair, *Colloids and Surfaces* **34**, 215 (1988/89).
- [98] H.J Taunton, C. Toprakcioglu, L.J. Fetters, and J. Klein, *Macromolecules* **23**, 571 (1990).
- [99] H. Dhoot, S. Watanabe, and M. Tirrell, *Colloids and Surfaces* **A.86**, 47 (1994).
- [100] T. Cosgrove, T. Heath, J. Phipps, and R. Richardson *Macromolecules* **24**, 94 (1991).

- [101] A. Karim, S. Satija, J. Douglas, J. Ankner, and L. Fetters *Phys. Rev. Lett.* **73**, 3407 (1994).
- [102] B.J. Factor, L.T. Lee, M. S. Kent, and F. Rondelez, *Phys. Rev. E* **48**, 2354 (1993).
- [103] E. Helfand, *J. Chem. Phys.* **62**, 999 (1975).
- [104] T. Ohta and K. Kawasaki, *Macromolecules* **19**, 2621 (1986).
- [105] M. Banaszak, Ph.D. thesis, Memorial University of Newfoundland, 1991.
- [106] K.F. Freed, *Renormalization Group Theory of Macromolecules* (John Wiley & Sons, New York, 1987).
- [107] P.J. Flory, *Principles of Polymer Chemistry* (Cornell Univ. Press, Ithaca, NY, 1953), p.509
- [108] R. Ober, L. Paz, C. Taupin, P. Pincus. and S. Boileau *Macromolecules* **16**, 50 (1983)
- [109] Z.Y. Chen, J. Noolandi, and D. Izzo, *Phys. Rev. Lett.* **66**, 727 (1991).
- [110] I. Jones and P. Richmond, *J. Chem. Soc., Faraday Trans. 2* **73**, 1062 (1977)
- [111] M.P. Pépin, and M.D. Whitmore, *J. Chem. Phys.* **111**, 10381 (1999)



